Inorganic Chemistry
Article

Inorg. Chem. **2010**, *49*, 3387–3401 **3387**
DOI: 10.1021/ic902516r

Mössbauer, Electron Paramagnetic Resonance, and Magnetic Susceptibility Studies on Members of a New Family of Cyano-Bridged 3d-4f Complexes. Demonstration of Anisotropic Exchange in a Fe−Gd Complex

Sebastian A. Stoian,[‡] Carmen Paraschiv,[†] Nathalie Kiritsakas,[§] Francesc Lloret,[∥] Eckard Münck,*[,‡] Emile L. Bominaar,*[,‡] and Marius Andruh*[,†]

[†]*Inorganic Chemistry Laboratory, Faculty of Chemistry, University of Bucharest, Str. Dumbrava Rosie nr. 23, 020464 Bucharest, Romania,* [‡]*Department of Chemistry, Carnegie Mellon University, 4400 Fifth Avenue, Pittsburgh, Pennsylvania 15213,* [§]*Laboratoire de Chimie de Coordination Organique, UMR CNRS 7140, Université Louis Pasteur, F-67000, Strasbourg, France, and* [∥] *Departamento de Química Inorgànica/Instituto de Ciencia Molecular (ICMoL), Universitat de València, Polígono La Coma s/n, 46980 Paterna, València, Spain*

Received December 17, 2009

The synthesis and crystallographic characterization of a new family of M(μ-CN)Ln complexes are reported. Two structural series have been prepared by reacting in water rare earth nitrates (Ln^{III} = La, Pr, Nd, Sm, Eu, Gd, Dy, Ho) with $K_3[M(CN)_6]$ (M^{III} = Fe, Co) in the presence of hexamethylenetetramine (hmt). The first series consists of six isomorphous heterobinuclear complexes, $[(CN)_5M\text{-}CN\text{-}Ln(H_2O)_8]\cdot 2hmt$ ([FeLa] **1**, [FePr] **2**, [FeNd] **3**, [FeSm] **4**, [FeEu] **5**, [FeGd] **6**), while the second series consists of four isostructural ionic complexes, $[M(CN)_6][Ln(H_2O)_8]\cdot hmt$ ([FeDy] **7**, [FeHo] **8**, [CoEu] **9**, [CoGd] **10**). The hexamethylenetetramine molecules contribute to the stabilization of the crystals by participating in an extended network of hydrogen bond interactions. In both series the aqua ligands are hydrogen bonded to the nitrogen atoms from both the terminal CN^- groups and the hmt molecules. The [FeGd] complex has been analyzed with ^{57}Fe Mössbauer spectroscopy and magnetic susceptibility measurements. We have also analyzed the [FeLa] complex, in which the paramagnetic Gd^{III} is replaced by diamagnetic La^{III}, with ^{57}Fe Mössbauer spectroscopy, electron paramagnetic resonance (EPR), and magnetic susceptibility measurements, to obtain information about the low-spin Fe^{III} site that is not accessible in the presence of a paramagnetic ion at the complementary site. For the same reason, the [CoGd] complex, containing diamagnetic Co^{III}, was studied with EPR and magnetic susceptibility measurements, which confirmed the $S = 7/2$ spin of Gd^{III}. Prior knowledge about the paramagnetic sites in [FeGd] allows a detailed analysis of the exchange interactions between them. In particular, the question of whether the exchange interaction in [FeGd] is isotropic or anisotropic has been addressed. Standard variable-temperature magnetic susceptibility measurements provide only the value for a linear combination of J_x, J_y, and J_z but contain no information about the values of the individual exchange parameters J_x, J_y, and J_z. In contrast, the spin-Hamiltonian analysis of the variable-field, variable-temperature Mössbauer spectra reveals an exquisite sensitivity on the anisotropic exchange parameters. Analysis of these dependencies in conjunction with adopting the g-values obtained for [FeLa], yielded the values $J_x = +0.11$ cm^{-1}, $J_y = +0.33$ cm^{-1}, and $J_z = +1.20$ cm^{-1} ($\mathbf{S}_1\cdot J\cdot \mathbf{S}_2$ convention). The consistency of these results with magnetic susceptibility data is analyzed. The exchange anisotropy is rooted in the spatial anisotropy of the low-spin Fe^{III} ion. The condition for anisotropic exchange is the presence of low-lying orbital excited states at the ferric site that (i) effectively interact through spin−orbit coupling with the orbital ground state and (ii) have an exchange parameter with the Gd site with a value different from that for the ground state. Density functional theory (DFT) calculations, without spin−orbit coupling, reveal that the unpaired electron of the t_{2g}^5 ground configuration of the Fe^{III} ion occupies the *xy* orbital, that is, the orbital along the plane perpendicular to the Fe···Gd vector. The exchange-coupling constants for this orbital, j_{xy}, and for the other t_{2g} orbitals, j_{yz} and j_{xz}, have been determined using a theoretical model that relates them to the anisotropic exchange parameters and the g-values of Fe^{III}. The resulting values, $j_{yz} = -5.7$ cm^{-1}, $j_{xz} = -4.9$ cm^{-1}, and $j_{xy} = +0.3$ cm^{-1} are quite different. The origin of the difference is briefly discussed.

1. Introduction

Lanthanides can carry large spin ($S \leq 7/2$) and orbital ($L \leq 6$) moments, which makes them promising candidates for application in the design of magnetic materials.[1] However, the exchange interactions between the ions in polynuclear lanthanide complexes are small because the open 4f shells are shielded by full 4d shells. Stronger exchange interactions are likely to occur when lanthanide ions (Ln) are brought in

*To whom correspondence should be addressed. E-mail: emunck@cmu.edu (E.M.), eb7g@andrew.cmu.edu (E.L.B.), marius.andruh@dnt.ro (M.A.).

(1) Benelli, C.; Gatteschi, D. *Chem. Rev.* **2002**, *102*, 2369.

Published on Web 03/12/2010

contact with the unshielded open shells of 3d transition metal ions (M),[2] suggesting that mixed 3d-4f metal compounds may sustain magnetic ordering at more elevated temperatures than pure 4f compounds.[3]

Two families of mixed 3d-4f metal compounds have been reported: (a) compounds with Schiff-base ligands, containing $M(\mu\text{-}O)_2Ln$ bridges,[4−6] and (b) cyano-bridged compounds, which use $[M(CN)_6]^{3-}$ units as building blocks.[7−13] These compounds have been crystallized either as discrete molecules or as part of extended *n*-dimensional lattices.[1] Considerable effort has been devoted to determining the exchange interactions in these systems,[2] with the discrete species, notably the binuclear [MLn] complexes, being the preferred targets of these studies since the theory for describing their magnetic properties is simpler and more developed than for infinite lattices. These physical studies rely almost exclusively on magnetic susceptibility (χ) measurements as a function of temperature and on the isotropic exchange coupling Hamiltonian, $J_{iso}\hat{\mathbf{S}}_M\cdot\hat{\mathbf{S}}_{Ln}$, for the interpretation of the data. The sign of J_{iso} (a negative sign yields a ground state in which the spins of M and Ln are ordered ferromagnetically, while a positive sign gives an antiferromagnetically ordered ground state) have been gleaned from χT versus T curves: when χT increases (decreases) as a function of decreasing temperature, the coupling is ferromagnetic (antiferromagnetic).

Quantitative analysis of the exchange interactions in 3d-4f complexes faces two problems: (i) the temperature dependence of χT depends not only on *intra*-molecular exchange but also on *inter*-molecular exchange. We will show that the intra- and intermolecular interactions yield indistinguishable contributions to χT, under the condition that J_{intra}, $J_{inter} \ll k_BT$. (ii) There are "local" contributions to the temperature dependence of χT because of thermal population of low-lying excited states of the metal ions, in particular Stark levels of the lanthanide ions, that carry magnetic moments different from those of the ground states.[1,14] The local contributions have been estimated from magnetic studies of auxiliary compounds that are structurally congruent with the original compound ($M_{para}Ln_{para}$) but with the paramagnetic 3d site (M_{para}) being substituted by a diamagnetic 3d metal (M_{dia}).[6c,12c,13d,e] Magnetic measurements on the $M_{dia}Ln_{para}$ complexes provide the local contributions to χT associated with the lanthanide ions. Thus, by taking the difference $[\chi(M_{para}Ln_{para}) - \chi(M_{dia}Ln_{para})]T$ one obtains a quantity whose temperature dependence is free of the local Ln contributions and exclusively dependent on exchange interactions (and possibly local contributions of the 3d ion, see below). We will show that, besides eliminating the local contribution, the subtraction has the additional advantage of partially removing the temperature dependence arising from intermolecular interactions.

The presence of unquenched orbital momentum raises the fundamental question of whether the isotropic Hamiltonian $J_{iso}\hat{\mathbf{S}}_M\cdot\hat{\mathbf{S}}_{Ln}$ provides a valid description of the exchange interactions in 3d-4f systems.[15] The action of spin−orbital coupling, $\zeta\sum_k \hat{\mathbf{l}}_k\cdot\hat{\mathbf{S}}_k$, results in the admixture of excited spin−orbital states with reversed spin into the wave functions of ground doublet, introducing spatial anisotropies in the exchange interaction, leading to Hamiltonians of the form $J_x\hat{S}_{M,x}\hat{S}_{Ln,x} + J_y\hat{S}_{M,y}\hat{S}_{Ln,y} + J_z\hat{S}_{M,z}\hat{S}_{Ln,z}$ with unequal values for the components J_x, J_y, and J_z, and to antisymmetric exchange $\mathbf{d}\cdot(\hat{\mathbf{S}}_M\times\hat{\mathbf{S}}_{Ln})$, where the coupling constants are the components vector $\mathbf{d}$.[15] A notable exception is the Gd^{III} ion, which, because of its half-filled $4f^7$ shell, has vanishing orbital momentum. Not surprisingly, most quantitative analyses of 3d-4f exchange have been performed for Gd^{III} complexes. Table 1 presents the isotropic exchange coupling constants reported for [MGd] species.

A number of observations can be made from the data in Table 1. With a few exceptions, the reported couplings are ferromagnetic in the oxygen bridged complexes and, with one

(2) (a) Sessoli, R.; Powell, A. K. *Coord. Chem. Rev.* **2009**, *253*, 2328. (b) Andruh, M.; Costes, J.-P.; Diaz, C.; Gao, S. *Inorg. Chem.* **2009**, *48*, 3342.
(3) (a) Bartolome, F.; Bartolome, J.; Oushoorn, R. L.; Guillou, O.; Kahn, O. *J. Magn. Magn. Mater.* **1995**, *140−144*, 1711. (b) Evanghelisti, M.; Bartolome, F.; Bartolome, J.; Kahn, M. L.; Kahn, O. *J. Magn. Magn. Mater.* **1999**, *196−197*, 584.
(4) (a) Bencini, A.; Benelli, C.; Caneschi, A.; Carlin, R. L.; Dei, A.; Gatteschi, D. *J. Am. Chem. Soc.* **1985**, *107*, 8128. (b) Bencini, A.; Benelli, C.; Caneschi, A.; Dei, A.; Gatteschi, D. *Inorg. Chem.* **1986**, *25*, 572.
(5) (a) Benelli, C.; Caneschi, A.; Gatteschi, D.; Guillou, O.; Pardi, L. *Inorg. Chem.* **1990**, *29*, 1750. (b) Andruh, M.; Ramade, I.; Codjovi, E.; Guillou, O.; Kahn, O.; Trombe, J. C. *J. Am. Chem. Soc.* **1993**, *115*, 1822. (c) Costes, J.-P.; Dahan, F.; Dupuis, A.; Laurent, J.-P. *Inorg. Chem.* **1996**, *35*, 2400. (d) Costes, J.-P.; Dahan, F.; Dupuis, A.; Laurent, J.-P. *Inorg. Chem.* **1997**, *36*, 3429. (e) Costes, J.-P.; Dahan, F.; Dupuis, A. *Inorg. Chem.* **2000**, *39*, 5994. (f) Ramade, I.; Kahn, O.; Jeannin, Y.; Robert, F. *Inorg. Chem.* **1997**, *36*, 930. (g) Costes, J.-P.; Dahan, F.; Dupuis, A.; Laurent, J.-P. *New J. Chem.* **1998**, 1525. (h) Costes, J.-P.; Dahan, F.; Dupuis, A. *Inorg. Chem.* **2000**, *39*, 165. (i) Brewer, C.; Brewer, G.; Scheidt, W. R.; Shang, M.; Carpenter, E. E. *Inorg. Chim. Acta* **2001**, *313*, 65. (j) Costes, J.-P.; Dahan, F.; Dupuis, A.; Laurent, J.-P. *Inorg. Chem.* **2000**, *39*, 169.
(6) (a) Costes, J.-P.; Dahan, F.; Garcia-Tojal, J. *Chem.—Eur. J.* **2002**, *8*, 5430. (b) Costes, J.-P.; Clemente-Juan, J. M.; Dahan, F.; Dumestre, F.; Tuchagues, J.-P. *Inorg. Chem.* **2002**, *41*, 2886. (c) Costes, J.-P.; Dupuis, A.; Laurent, J. P. *J. Chem. Soc., Dalton Trans.* **1998**, 735. (d) Costes, J.-P.; Dahan, F.; Donnadieu, B.; Garcia-Tojal, J.; Laurent, J. P. *Eur. J. Inorg. Chem.* **2001**, 363. (e) Costes, J.-P.; Dahan, F.; Donnadieu, B.; Fernandez-Garcia, M. I.; Rodriguez-Douton, M. J. *Dalton Trans.* **2003**, 3776. (f) Costes, J.-P.; Dahan, F.; Dumestre, F.; Clemente-Juan, J. M.; Tuchagues, J.-P. *Dalton Trans.* **2003**, 464. (g) Costes, J.-P.; Dupuis, A.; Laurent, J. P. *Eur. J. Inorg. Chem.* **1998**, 1543. (h) Costes, J.-P.; Dahan, F.; Dupuis, A.; Laurent, J. P. *Chem.—Eur. J.* **1998**, *4*, 1616. (i) Sanz, J. L.; Ruiz, R.; Gleizes, A.; Lloret, F.; Faus, J.; Julve, M.; Borràs-Almanar, J. J.; Journaux, Y. *Inorg. Chem.* **1996**, *35*, 7384. (j) Costes, J.-P.; Dahan, F.; Dupuis, A.; Laurent, J.-P. *Inorg. Chem.* **1997**, *36*, 4284. (k) Chen, Q. Y.; Luo, Q. H.; Zheng, L. M.; Wang, Z. L.; Chen, J. T. *Inorg. Chem.* **2002**, *41*, 605.
(7) (a) Yan, B.; Chen, Z. *Chem. Lett.* **2000**, 1244. (b) Yan, B.; Chen, Z.; Wang, S.; Gao, S. *Chem. Lett.* **2001**, 350. (c) Yan, B.; Wang, H.-D.; Chen, Z.-D. *Polyhedron* **2001**, *20*, 591. (d) Yan, B.; Wang, H.-D.; Chen, Z.-D. *Inorg. Chem. Commun.* **2000**, *3*, 653. (e) Yan, B.; Chen, Z. *Helv. Chim. Acta* **2001**, *84*, 817.
(8) (a) Figuerola, A.; Diaz, C.; Ribas, J.; Tangoulis, V.; Granell, J.; Lloret, F.; Mahia, J.; Maestro, M. *Inorg. Chem.* **2003**, *42*, 641. (b) Sun, X.-R.; Chen, Z.-D.; Gao, S.; Cheung, K.-K.; Che, C.-M.; Zhang, X.-X. *J. Cluster Sci.* **2002**, *13*, 103.
(9) Plecnik, C. E.; Liu, S.; Shore, S. G. *Acc. Chem. Res.* **2003**, *36*, 499.
(10) Zhao, H.; Lopez, N.; Prosvirin, A.; Chifotides, H. T.; Dunbar, K. R. *Dalton Trans.* **2007**, 878.
(11) Tanase, S.; Andruh, M.; Müller, A.; Schmidtmann, M.; Mathonière, C.; Rombaut, G. *Chem. Commun.* **2001**, 1084.
(12) (a) Kou, H.-Z.; Gao, S.; Sun, B.-W.; Zhang, J. *Chem. Mater.* **2001**, *13*, 1431. (b) Kou, H.-Z.; Gao, S.; Jin, X. *Inorg. Chem.* **2001**, *40*, 6295. (c) Ma, B.-Q.; Gao, S.; Su, G.; Xu, G.-X. *Angew. Chem., Int. Ed.* **2001**, *40*, 434. (d) Gao, S.; Su, G.; Yi, T.; Ma, B.-Q. *Phys. Rev. B* **2001**, *63*, 054431. (e) Yan, F.; Chen, Z. D. *J. Phys. Chem. A* **2000**, *104*, 6295.
(13) (a) Figuerola, A.; Ribas, J.; Solans, X.; Font-Bardía, M.; Maestro, M.; Diaz, C. *Eur. J. Inorg. Chem.* **2006**, 1846. (b) Figuerola, A.; Diaz, C.; El Fallah, M. S.; Ribas, J.; Maestro, M.; Mahia, J. *Chem. Commun.* **2001**, 1204. (c) Figuerola, A.; Diaz, C.; Ribas, J.; Tangoulis, V.; Sangregorio, C.; Gatteschi, D.; Maestro, M.; Mahia, J. *Inorg. Chem.* **2003**, *42*, 5274. (d) Figuerola, A.; Ribas, J.; Casanova, D.; Maestro, M.; Alvarez, S.; Diaz, C. *Inorg. Chem.* **2005**, *44*, 6949. (e) Estrader, M.; Ribas, J.; Tangoulis, V.; Solans, M.; Font-Bardia, M.; Maestro, M.; Diaz, C. *Inorg. Chem.* **2006**, *45*, 8239.
(14) (a) Kahn, M. L.; Mathonière, C.; Kahn, O. *Inorg. Chem.* **1999**, *38*, 3692. (b) Sutter, J.-P.; Kahn, M. L. In *Magnetism: Molecules to Materials*; Miller, J. S., Drillon, M., Eds.; Wiley-VCH: Weinheim, Germany, 2005; Vol. *V*, p 161, and references therein.
(15) Bencini, A.; Gatteschi, D. *EPR of Exchange Coupled Systems*; Springer-Verlag: Berlin, Germany, 1990.

Table 1. Effective Exchange-Coupling Constants Reported for M−Gd Bridges in Discrete Complexes Obtained from Magnetic Susceptibility Measurements with Isotropic Exchange Hamiltonian

bridges[a]	J_χ (cm^{-1})[b]	reference
$[V^{IV}{=}O](\mu\text{-}O)_2Gd$	−1.3	6c
$[V^{IV}{=}O](\mu\text{-}O)_2Gd$	+2.6	6d
$Fe^{III}{}_{HS}(\mu\text{-}O)_2Gd$[c]	+1.4[c]	6f
$Fe^{III}{}_{HS}(\mu\text{-}O)_3Gd$	−0.50	6g
$Fe^{II}{}_{HS}(\mu\text{-}O)_2Gd$[d]	−1.0	6b
$Fe^{II}{}_{HS}(\mu\text{-}O)_2Gd$[d]	−0.82	6b
$Fe^{II}{}_{HS}(\mu\text{-}O)_2Gd$[d]	−0.16	6b
$Co^{II}(\mu\text{-}O)_2Gd$[e]	−0.90	6a
$Ni^{II}(\mu\text{-}O)_2Gd$	−3.6	6j
$Ni^{II}(\mu\text{-}O)_2Gd$	−0.6	6k
$Cu^{II}(\mu\text{-}O)_2Gd$[f]	−5.3	4a
$Cu^{II}(\mu\text{-}O)_2Gd$[g]	−7.4	4a
$Cu^{II}(\mu\text{-}O)_2Gd$[h]	−1.2	4b
$Cu^{II}(\mu\text{-}O)_2Gd$[i]	−2.5	5a
$Cu^{II}(\mu\text{-}O)_2Gd$[j]	−6.0	5b
$Cu^{II}(\mu\text{-}O)_2Gd$	−7.0	5c
$Cu^{II}(\mu\text{-}O)_2Gd$	−1.4	5g
$Cu^{II}(\mu\text{-}O)_2Gd$	−5.0	5d
$Cu^{II}(\mu\text{-}O)_2Gd$	−6.8	5d
$Cu^{II}(\mu\text{-}O)_2Gd$	−7.2	5d
$Cu^{II}(\mu\text{-}O)_2Gd$	−4.8	5d
$Cu^{II}(\mu\text{-}O)_2Gd$	−4.2	5h
$Cu^{II}(\mu\text{-}O)_2Gd$	−10.1	5i
$Cu^{II}(\mu\text{-}O)_2Gd$	−1.9	5j
$Cu^{II}(\mu\text{-}O)(\mu\text{-}NO)Gd$	−3.5	5k
$Cu^{II}(\mu\text{-}O)(\mu\text{-}NO)Gd$	+0.5	5k
$Cu^{II}(\mu\text{-}N_2C_2O_2)Gd$[k]	−0.9	6i
$Cr^{III}(\mu\text{-}CN)Gd$[l]	+0.5	13b
$Cr^{III}(\mu\text{-}CN)Gd$[l]	+1.1	13b
$Cr^{III}(\mu\text{-}CN)Gd$	−0.8	12e
$Fe^{III}{}_{LS}(\mu\text{-}CN)Gd$	−1.5[m]	8b
$Fe^{III}{}_{LS}(\mu\text{-}CN)Gd$[l]	+0.8	13c
$Fe^{III}{}_{LS}(\mu\text{-}CN)Gd$	+0.5	this work

[a] Spins: V^{IV} ($S = 1/2$), Cr^{III} ($S = 3/2$), Fe^{II} (HS is $S = 2$), Fe^{III} (LS is $S = 1/2$; HS is $S = 5/2$), Co^{II} ($S = 3/2$), Ni^{II} ($S = 1$), Cu^{II} ($S = 1/2$), and Gd^{III} ($S = 7/2$); bridging groups are given in parentheses. Dinuclear complexes if not indicated otherwise. [b] $JS_1 \cdot S_2$ convention. [c] $GdFe_2Gd$ complex; $J_{FeFe} = 203\ cm^{-1}$. Antiferromagnetic sign of J has not been unequivocally confirmed. [d] $D_{Fe} = 2.1, 3.2$, and $4.4\ cm^{-1}$ respectively; HS is $S = 2$. [e] Zero-field splitting $D_{Fe} = 4.2\ cm^{-1}$. [f] Cu_2Gd complex; $J_{CuCu} = +4.2\ cm^{-1}$. [g] Cu_2Gd complex; $J_{CuCu} = +12.2\ cm^{-1}$. [h] Cu_2Gd complex; $J_{CuCu} = +3.6\ cm^{-1}$. [i] Cu_2Gd_2 complex; $J_{CuCu} = 0\ cm^{-1}$ and $J_{GdGd} = +0.9\ cm^{-1}$. [j] Cu_4Gd_2 complex. $J_{CuCu} = +3.1\ cm^{-1}$, as obtained for Cu_4La_2, and $J'_{CuCu} = 0$ have been imposed in fit. [k] Cu_2GdCu_2 complex; $J_{CuCu} = 0.4\ cm^{-1}$. [l] One-dimensional chain. [m] This value is ambiguous, see discussion.

exception, antiferromagnetic in the cyano-bridged species. The magnitude of J_{iso} in the first group of complexes is typically larger than in the second group, especially for the copper complexes. The variations in the J_{iso} values suggest that this quantity depends on a host of factors, including the type of ligand bridge, the metal and its (spin/oxidation) state, and details of the structure of the bridging unit. For example, the data for the [CuGd] complexes reveals a magneto−structural correlation between J_{iso} and dihedral angle Cu-$(\mu\text{-}O)_2Gd$.[5d] Among the J_{iso} values listed, the most reliable numbers are those obtained for the discrete binuclear complexes. Species of higher nuclearity (see footnotes of Table 1) require fits with more than one adjustable exchange-coupling constant, introducing a source of ambiguity in the results.

Although the quality of the χT fits obtained with the isotropic exchange-coupling constants listed in Table 1 is excellent, the agreement does *not* imply that the exchange interactions in these systems are isotropic. We will demonstrate that the χ versus T data of randomly oriented samples recorded for $T \gg J_{x,y,z}/k_B$ depend only on a linear combination of J_x, J_y, and J_z and contain no information about the values of the individual components.

The lanthanide ion in 3d-4f complexes is not necessarily the only source of exchange anisotropy: the spin−orbit coupling between the ground and excited crystal-field states of the 3d site may also give rise to this type of interaction. Low spin Fe^{III}, such as present in ferricyanide, has a highly anisotropic set of g values and a temperature dependent χT,[16] arising from spin−orbit interactions within a weakly crystal-field split $^2T_2$ manifold, creating suitable conditions for generating 3d-based exchange anisotropies. Table 1 shows that cyano-bridged, low-spin $Fe^{III}-Gd^{III}$ complexes are, indeed, available but few in number.

In this paper we report two new families of cyano-bridged complexes, which were obtained by reacting rare earth nitrates (Ln = La, Pr, Nd, Sm, Eu, Gd, Dy, Ho) with $K_3[M(CN)_6]$ ($M = Co^{III}$, Fe^{III}) in the presence of hexamethylenetetramine (htm). The first family consists of six isomorphous cyano-bridged heterobinuclear complexes, $[(H_2O)_8Ln\text{-}NC\text{-}M(CN)_5]\cdot 2hmt$ ([FeLa] **1**, [FePr] **2**, [FeNd] **3**, [FeSm] **4**, [FeEu] **5**, [FeGd] **6**), while the second one consists of four isostructural ionic complexes, $[Ln(H_2O)_8][M(CN)_6]\cdot hmt$ ([FeDy] **7**, [FeHo] **8**, [CoEu] **9**, [CoGd] **10**). The structures of the two families will be discussed. Complexes **6**, **1**, and **10**, representing the structurally congruent species $M_{para}Ln_{para}$, $M_{para}Ln_{dia}$, and $M_{dia}Ln_{para}$ introduced above, have been selected for spectroscopic analysis.

The physical analysis has been organized as follows. First, we performed χ versus T measurements on the Fe(μ-CN)Gd complex (**6**) and the auxiliary complexes Fe(μ-CN)La (**1**) and Co(μ-CN)Gd (**10**). As expected for a nearly ideal Curie-type paramagnet, χT of **10** is independent of the temperature for $T > 2$ K, while χT of **1** showed pronounced temperature dependence. The local contribution of the low-spin Fe^{III} site in **6** was removed by taking the difference $[\chi(FeGd) - \chi(FeLa)]T$. The temperature dependence of this difference was analyzed using the isotropic exchange Hamiltonian, which yielded an antiferromagnetic exchange-coupling constant, $J_\chi \approx 0.5\ cm^{-1}$. It is shown that J_χ cannot be identified with the isotropic part of the exchange interaction, J_{iso}. Second, we performed electron paramagnetic resonance (EPR) measurements of the [FeLa] **1** and [CoGd] **10** complexes. As anticipated, the g values for **10** showed only minor deviations from the free electron value, while those for **1** exhibited a significant degree of anisotropy similar to that observed in ferricyanide. Third, we recorded ^{57}Fe Mössbauer spectra of the iron-containing species **6** and **1** for a wide range of temperatures and applied magnetic field strengths. These measurements probe the electronic structure of the [FeGd] dimer in **6** from the perspective of the iron nucleus, revealing details about the exchange interaction that were inaccessible by χT measurements. The full set of variable-temperature, variable-field spectra were simulated by using the standard spin-Hamiltonian technique. The Mössbauer simulations confirmed the result of the magnetic susceptibility analysis that the exchange in **6** is antiferromagnetic. However, the Mössbauer simulations made under the assumption of

(16) (a) Baker, J. M.; Bleaney, B.; Bowers, K. D. *Proc. Phys. Soc* (*London*) **1956**, *B69*, 1205. (b) Bleaney, B.; O'Brien, M. C. M. *Proc. Phys. Soc*. (*London*) **1956**, *B69*, 1216.

isotropic exchange yielded for J_{iso} twice the magnitude deduced from the magnetic susceptibility analysis and failed to reproduce some of the salient features of the low-temperature, low-field spectra. The inconsistency was resolved by relaxing the isotropy constraint on the exchange and thus, we obtained excellent simulations for the full set of spectra by allowing for different values for J_x, J_y, and J_z. Determination of these components required prior knowledge of g-values of the Fe site, for which we adopted the EPR values as obtained for **1**, illustrating the utility of combining information from complementary techniques.

Finally, the anisotropy of the exchange interaction in **6** is interpreted in terms of exchange pathways between the t_{2g} orbitals of Fe and the 4f shell of Gd, using DFT calculations, and the resulting exchange pathway parameters are discussed in the context of the data presented in Table 1.

2. Materials and Methods

All the chemicals used for the present study were purchased from commercial sources and used without any further purification. The preparation method is general: the 10 compounds were obtained by slow diffusion, in H-shaped tubes, of two aqueous solutions, one of them containing a mixture of $Ln(NO_3)_3 \cdot nH_2O$ and hexamethylenetetramine, and the other one $K_3[M(CN)_6]$, in 1:1:1 molar ratio. Well-formed single crystals formed for all of them after 2 months. Their colors vary from orange via yellow to colorless, depending on the 3d-4f pair.

X-ray diffraction measurements for **1** were performed on a Bruker SMART CCD Diffractometer, using graphite-monochromated Mo-Kα radiation (λ = 0.71073 Å). Diffraction data were corrected for absorption and analyzed using the OpenMolen package.[17] All non-H atoms were refined anisotropically. Hydrogen atoms were introduced as fixed contributors at calculated positions (C−H 0.95 Å, B(H) = 1.3Beq). Final difference maps revealed no significant maxima. The X-ray single crystal measurements for **7** were carried out using a STOE IPDS with graphite-monochromated Mo−Kα radiation (λ = 0.71069 Å). The structures were solved by direct methods (SHELXS) and refined by full-matrix least-squares (SHELXL).[18] The hydrogen atoms were included at idealized positions and not refined (riding model). A summary of the crystallographic data and the structure refinement is given in Table 2. The cell constants for the isostructural compounds **1**−**6** and **7**−**10** are gathered in Table 3.

Magnetic susceptibility measurements on polycrystalline samples of **1** and **6** were carried out with a Quantum Design SQUID magnetometer in the temperature range 2−300 K in an applied magnetic field from 0.02 to 1.0 T. Diamagnetic corrections of the constituent atoms were estimated from Pascal constants.

Mössbauer spectra were collected on constant acceleration instruments at temperatures between 2 and 150 K in applied external fields up to 8 T. Simulations of spectra were generated using WMOSS (WEB Research, Edina, MN) as well as a modified version of SPHMOSS (Sp*in*H*amiltonian*Möss*bauer*).[19] Isomer shifts are reported relative to iron metal foil at room temperature. The Mössbauer samples were prepared from crystalline and amorphous powders and were contained in Teflon cups covered with Teflon lids.

Table 2. Crystallographic Data, Details of Data Collection, and Structure Refinement Parameters for Compounds **1** and **7**

	1	**7**
chemical formula	C18H24FeLaN14O8	C18H24DyFeN14O8
M (g mol^{-1})	759.27	782.86
temperature (K)	173(2)	293(2)
wavelength (Å)	0.71073	0.71073
crystal system	monoclinic	cubic
space group	$P2_1/c$	$Fm\bar{3}m$
a (Å)	14.9250(4)	14.6477(16)
b (Å)	10.1240(2)	14.6477(16)
c (Å)	20.2330(5)	14.6477(16)
α (deg)	90	90.00
β (deg)	91.2330(12)	90.00
γ (deg)	90	90.00
V (Å^3)	3056.51(13)	3142.7(6)
Z	4	4
D_c (g cm^{-3})	1.650	1.655
μ (mm^{-1})	1.917	2.882
F(000)	1508	1544
goodness-of-fit on F^2	1.016	1.197
final R1, wR2 [$I > 2\sigma(I)$]	0.0531, 0.1233	0.0261, 0.0623
R1, wR2 (all data)	0.0815, 0.1359	0.0261, 0.0623
Largest diff. peak and hole (e Å^{-3})	2.021 and −1.491	0.443 and −0.327

The EPR spectra were recorded using a Bruker EPR 300 spectrometer equipped with Oxford ESR 910 cryostat. The EPR spectra were analyzed using a program written by Dr. M. P. Hendrich at Carnegie Mellon University.[20] To avoid dealing with partially oriented samples, all the EPR spectra were prepared by precipitation.

Density Functional Theory (DFT) computations were performed using the quantum mechanical software package Gaussian '03. Single point calculations were performed on the crystallographic structures using the B3LYP functional and CEP-4G basis set. The SCF iterations were terminated after the default convergence criteria were fulfilled. The stability of the electronic ground state was checked using time-dependent (TD) DFT.

3. Results

3.1. Structural Characterization. The aggregation of polynuclear complexes within a $Ln(aq)^{3+}$−$[M(CN)_6]^{3-}$-ligand system is rather serendipitous. While in the case of the 3d assembling cations network topologies can be more easily controlled, the peculiarities of the lanthanide ions (high coordination numbers, low stereochemical preferences, and rather weak metal−ligand bonds) make the prediction of the final solid-state architectures difficult.[9,7,10−13]

In the self-assembly process involving lanthanide cations an important role is played by their ionic radii, which decrease along the series. Consequently, ligand−ligand repulsion in the lanthanide series is increasingly stronger and might lead to different structural types. Indeed, the reaction between rare earth nitrates and $K_3[Fe(CN)_6]$ in the presence of hexamethylenetetramine affords two series of complexes: $[(H_2O)_8Ln\text{-}NC\text{-}M(CN)_5] \cdot 2hmt$, for large lanthanide ions ([FeLa] **1**, [FePr] **2**, [FeNd] **3**, [FeSm] **4**, [FeEu] **5**, [FeGd] **6**; Type I), and

(17) *OpenMolenN, Interactive Structure Solution*; Nonius B. V.: Delft, The Netherlands, 1997.

(18) Sheldrick, G. M. *SHELXS-97, Crystal Structure Solution*, WinGX version, release 97-2; University of Göttingen: Göttingen, Germany, 1997.

(19) Münck, E.; Groves, J. L.; Tumolillo, T. A.; Debrunner, P. G. *Comput. Phys. Commun.* **1973**, *5*, 225.

(20) The program used for the simulation of the EPR spectra can be downloaded from: http://www.chem.cmu.edu/groups/hendrich/facilities/index.html

Table 3. Crystallographic Data for Compounds **1**−**10**

	1	2	3	4	5	6	7	8	9	10
a (Å)	14.9250(4)	14.9837	14.8760(4)	14.8330	14.910(3)	14.8880	14.6477(16)	14.6540	14.5905	14.5479(4)
b (Å)	10.1240(2)	10.0907	10.0620(2)	10.0130	10.044(2)	10.0010	14.6477(16)	14.6540	14.5905	14.5479(4)
c (Å)	20.2330(5)	20.2355	20.1290(5)	20.0040	20.068(4)	20.0270	14.6477(16)	14.6540	14.5905	14.5479(4)
α (deg)	90	90	90	90	90	90	90	90	90	90
β (deg)	91.2330(12)	91.126	91.3250(15)	88.55	91.19(3)	91.1600	90	90	90	90
γ (deg)	90	90	90	90	90	90	90	90	90	90

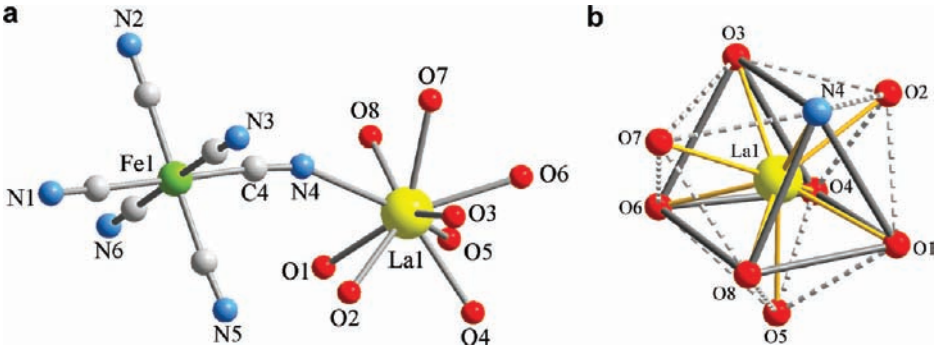

Figure 1. (a) View of the binuclear unit in crystal **1**, along with the atom numbering scheme; (b) the coordination environment around the lanthanum(III) ion.

$[Ln(H_2O)_8][M(CN)_6]\cdot$hmt for smaller lanthanide ions ([FeDy] **7**, [FeHo] **8**; Type II). We also synthesized two cobalt derivatives, [CoEu] **9**, [CoGd] **10**, which belong to the second structural type.

The two series of compounds are particularly interesting because of their remarkable simplicity: they are constructed solely from hydrated lanthanide ions and hexacyanometallate anions. The hexamethylenetetramine molecules play a decisive role in stabilizing the crystals, being involved in an extended network of hydrogen bond interactions.

3.1.1. Type I Structures. Single-crystal X-ray studies revealed that **1**−**6** are isostructural and crystallize in the monoclinic space group $P2_1/c$ (Table 2). Only the crystal structure of the lanthanum derivative will be described here. The molecular structure consists of a binuclear cyano-bridged $\{Fe^{III}-La^{III}\}$ unit and two non-coordinated hexamethylenetetramine molecules (Figure 1a). The lanthanum ion is nine-coordinated, being surrounded by the nitrogen atom of the cyano bridge and eight oxygen atoms from the coordinated water molecules. The coordination geometry of the lanthanum(III) ion can be best approximated as a tricapped trigonal prism, that is defined by O(1)O(4)O(6)-O(8)N(4)O(3), while O(2), O(5), and O(7) can be considered as the capping atoms (Figure 1b). The longest bond corresponds to the cyano bridge [La(1)−N(4) = 2.673(4) Å], while the La−O bond lengths vary from 2.529(4) to 2.613(3) Å. The cyano bridge deviates from linearity, with the La(1)−N(4)−C(4) angle being equal to 156.1(3)°.

The geometry of the $[Fe(CN)_6]^{3-}$ unit is a slightly distorted octahedron, with Fe−C bond lengths ranging from 1.927(5) to 1.953(5) Å (the highest value corresponds to the cyano bridge). The Fe−C−N angles are almost linear and range from 175.2(4) to 178.7(5)°. The intramolecular distance between Fe^{III} and La^{III} is 5.620 Å. Selected bond lengths and angles are listed in Table 4.

The water molecules coordinated to the La^{III} ion act as hydrogen bond donors toward the nitrogen atoms of the terminal CN^- ligands and from the non-coordinated hmt molecules, linking the components into a complex 3-D framework (Figure 2a). Five out of the eight water molecules form two hydrogen bonds, while the three others act as hydrogen bond donors toward only one nitrogen atom (Figure 2b). The five terminal cyano groups of the ferricyano moiety connect five adjacent binuclear $[Fe^{III}La^{III}]$ units, the N···O distances varying between 2.721 and 2.972 Å. Two of the cyano nitrogens, N(2) and N(3), form two hydrogen bonds, while each of the other three CN^- groups interact with one hydrogen of one coordinated water molecule (Figure 2c). Each hmt

Table 4. Selected Bond Lengths and Angles for **1** and **7**

1		**7**	
La(1)−O(1)	2.529(4)	Dy(1)−O(1)	2.309(9)
La(1)−O(2)	2.557(3)	Fe(2)−C(1)	1.918(9)
La(1)−O(3)	2.532(4)	N(1)−C(1)	1.137(14)
La(1)−O(4)	2.553(3)	N(2)−C(2)	1.465(4)
La(1)−O(5)	2.613(3)		
La(1)−O(6)	2.554(4)		
La(1)−O(7)	2.570(3)		
La(1)−O(8)	2.552(3)		
La(1)−N(4)	2.673(4)		
Fe(1)−C(1)	1.941(5)		
Fe(1)−C(2)	1.928(5)		
Fe(1)−C(3)	1.949(5)		
Fe(1)−C(4)	1.953(5)		
Fe(1)−C(5)	1.927(5)		
Fe(1)−C(6)	1.948(5)		
C(1)−N(1)	1.144(6)		
C(2)−N(2)	1.154(6)		
C(3)−N(3)	1.139(7)		
C(4)−N(4)	1.154(6)		
C(5)−N(5)	1.147(6)		
C(6)−N(6)	1.141(7)		
N(1)−C(1)−Fe(1)	178.0(5)		
N(2)−C(2)−Fe(1)	177.9(5)	N(1)−C(1)−Fe(2)	180.0
N(3)−C(3)−Fe(1)	177.6(5)		
N(4)−C(4)−Fe(1)	175.2(4)		
N(5)−C(5)−Fe(1)	175.5(5)		
N(6)−C(6)−Fe(1)	178.7(5)		
C(4)−N(4)−La(1)	156.1(3)		

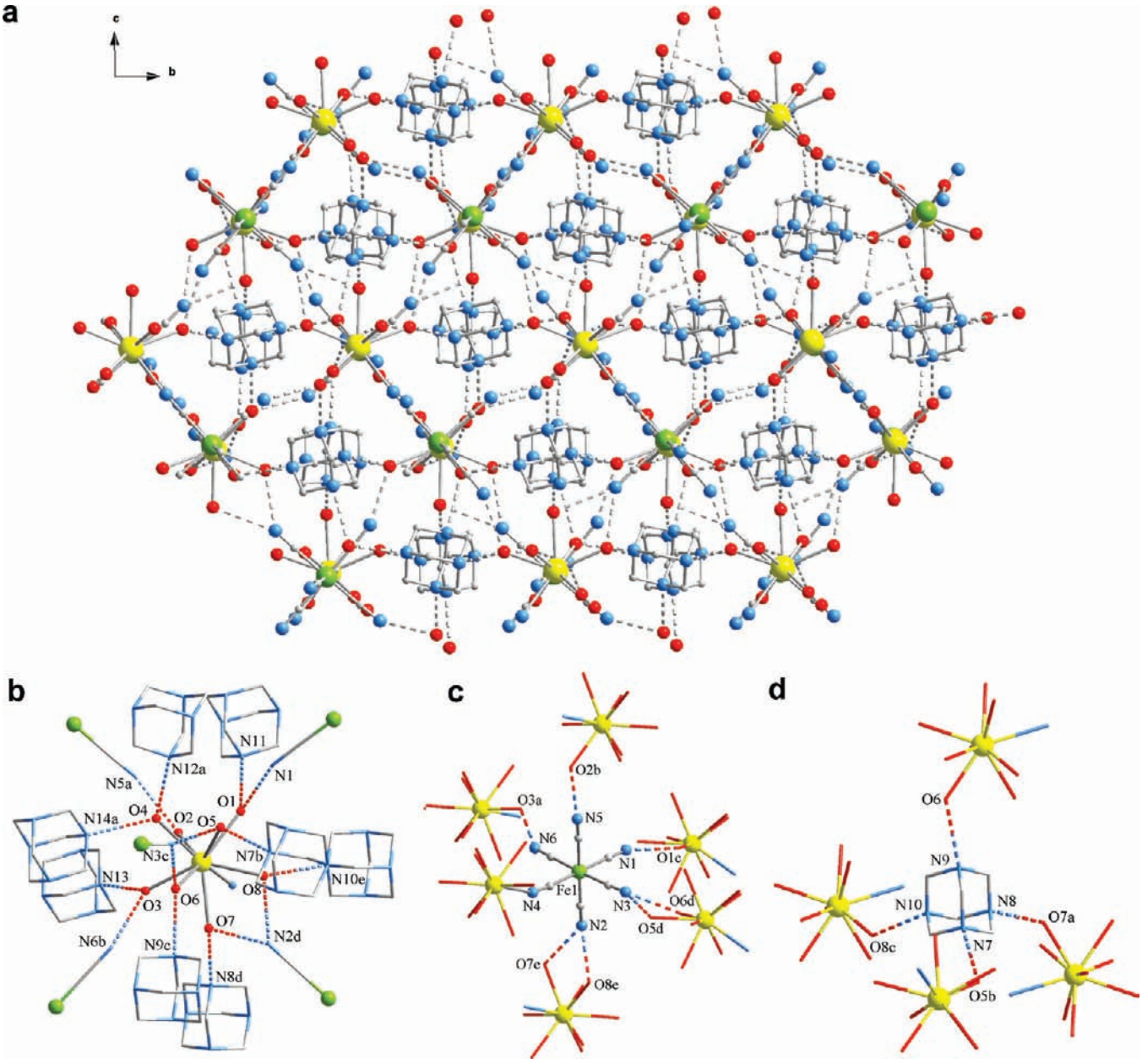

Figure 2. 3D supramolecular architecture in **1** (a), and details of the packing diagram showing the hydrogen bonds formed by the water molecules coordinated to the La^{III} ion (b), the ferricyano moiety with its second coordination sphere (c), and the hexamethylenetetramine molecules (d).

molecule interacts through hydrogen bonds with four bimetallic units, with N···O distances ranging from 2.745 to 2.929 Å (Figure 2d). The parameters of the hydrogen bonds are listed in Table 5.

3.1.2. Type II Structures. Compounds **7**−**10** were obtained using the same experimental conditions, and the crystallographic analyses revealed that they all are isomorphous and crystallize in the cubic space group $Fm\bar{3}m$ (Table 2). All of them exhibit a NaCl-type crystal structure (Figure 3a). Because of the decrease of the ionic radii in the lanthanide series, the small 4f ions present lower coordination numbers. Consequently, when using Dy^{III} or Ho^{III}, no cyano bridges are formed between the 3d and 4f metal centers. An ionic compound, complex cation−complex anion, is formed.

The crystal structure of [FeDy] **7** consists of $[Fe(CN)_6]^{3-}$ anions that alternate with $[Dy(H_2O)_8]^{3+}$ cations in the corners of a cube, the distance between the metallic centers being of 7.324 Å. The Dy^{III} ion is coordinated by eight aqua ligands and has a cubic environment, with the Dy−O distances of 2.309(9) Å. One non-coordinated hmt molecule is hosted inside each cube, being involved in hydrogen bond interactions with the aqua ligands of four different $[Dy(H_2O)_8]^{3+}$ entities. Each oxygen atom is disordered over three positions. Hydrogen bonds are formed between the coordinated water molecules and the nitrogen atoms from both the terminal CN^- groups and the hmt molecules, leading to a three-dimensional supramolecular architecture (Figure 3b).

3.2. Magnetic Susceptibilities of [FeLa] and [FeGd] Complexes. Curve A of Figure 4 presents the temperature dependence of $\chi_{FeGd}T$ for compound **6**. The $\chi_{FeGd}T$ versus T curve depends on four contributions: (i) A constant term, which is the sum of the Curie constants

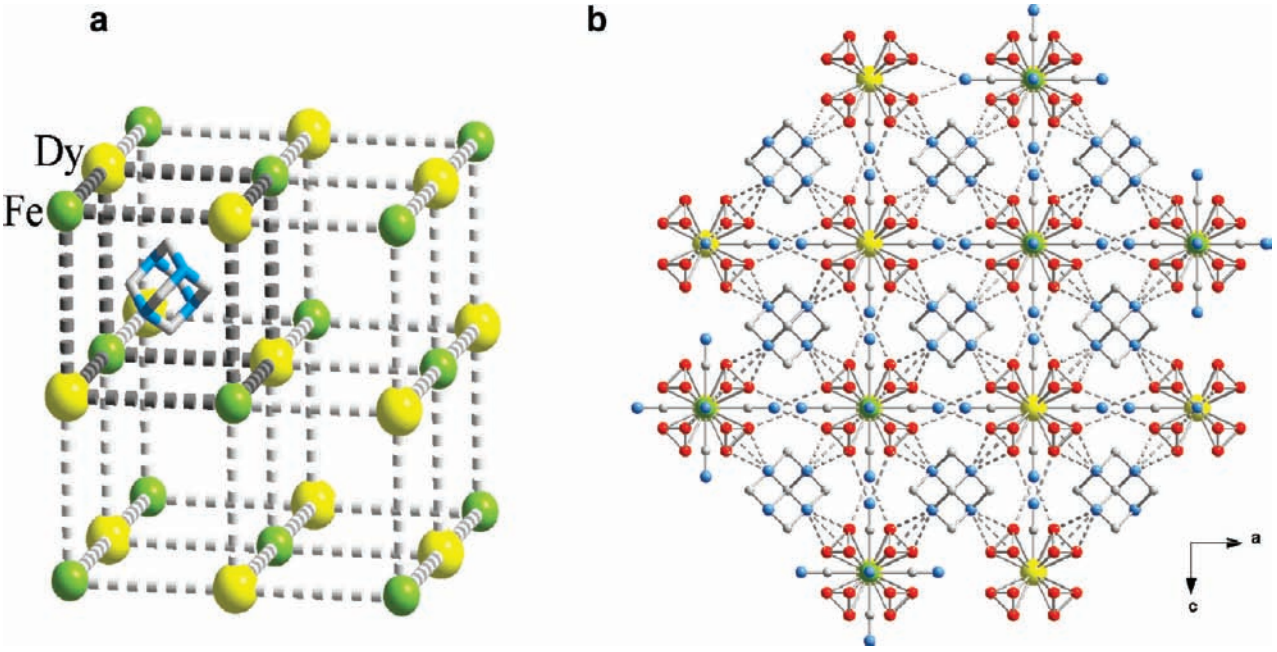

Figure 3. (a) NaCl type structure of compound **7**; (b) packing diagram showing the hydrogen bonds connecting the molecules.

Table 5. Geometrical Parameters of the Hydrogen Bonds in **1**

D···A (Å)	
O(1)···N(1)	2.768
O(1)···N(11)	2.877
O(2)···N(5)	2.721
O(3)···N(6)	2.779
O(3)···N(13)	2.894
O(4)···N(12)	2.929
O(4)···N(14)	2.823
O(5)···N(3)	2.972
O(5)···N(7)	2.853
O(6)···N(3)	2.831
O(6)···N(9)	2.833
O(7)···N(2)	2.845
O(7)···N(8)	2.769
O(8)···N(2)	2.820
O(8)···N(10)	2.745

for Gd^{III} and the ground state of Fe^{III}. (ii) A temperature-dependent, local Fe^{III} contribution, arising from thermally populating excited states with a larger magnetic moment than the ground state. The gradual increase in excited state population as a function of increasing temperature yields the steady rise of curve A above 50 K. The local contribution for the Fe^{III} site has been estimated from magnetic susceptibility measurements on [FeLa] complex **1** in which the paramagnetic Gd^{III} sites of **6** have been replaced by diamagnetic La^{III} ions. The $\chi_{FeLa}T$ versus T curve is presented in Figure S7 of the Supporting Information. If we assume that the magnetic properties of the Fe^{III} sites in **1** and **6** are identical, the local Fe^{III} contribution can be removed from the data for **6** by taking the difference, $\chi_{FeGd}T - \chi_{FeLa}T$. The difference curve (B in Figure 4) is, indeed, practically constant above 50 K, supporting the assumed identity. There remains, however, a small residual temperature dependence above 50 K, which is discussed in section II of the Supporting Information. (iii) A c/T term due to exchange interactions (J_{ij}) between the paramagnetic sites (i and j), where c is a coefficient, which is independent of temperature under the

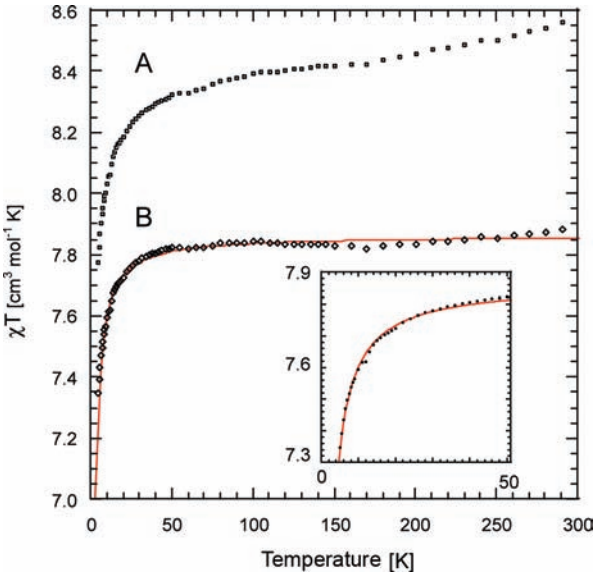

Figure 4. (A) $\chi_{FeGd}T$ versus T. (B) $(\chi_{FeGd} - \chi_{FeLa})T$ versus T. Inset: Curve B in 5−50 K range. Red curves are fits with function $c_1 - c_2/T$ in the temperature ranges shown.

condition that $|J_{ij}/k_BT| \ll 1$. Obviously, this term is large at low temperatures and vanishes in the high-temperature limit. The coefficient c is a linear combination of exchange-coupling constants, $c = \Sigma_{ij}c_{ij}J_{ij}$, including *intra*-molecular ($J = J_{FeGd}$) and *inter*-molecular ($J_{FeFe'}$, $J_{FeGd'}$, and $J_{GdGd'}$) interactions (see section I of the Supporting Information). Thus, intra- and intermolecular exchange interactions give indistinguishable contributions to the χT versus T curve. Noting, however, that the shortest Fe−Gd′ (7.4 Å) and Gd−Gd′ (9.2 Å) distances in **6** are considerably longer than the intramolecular Fe−Gd (5.6 Å) distance, we can safely assume that the contributions to $\chi_{FeGd}T$ from $J_{FeGd'}$ and $J_{GdGd'}$ are negligible compared to that of J. We have shown in the Supporting Information that if the

$J_{FeFe'}$ couplings in **1** and **6** are equal, the $c_{FeFe'}J_{FeFe'}/T$ terms drop from the difference $\chi_{FeGd}T - \chi_{FeLa}T$ (see eq S22). The difference has been written as follows:

$$(\chi_{FeGd} - \chi_{FeLa})T = 7.875 - 5.665\frac{J_\chi}{T} \qquad (1)$$

where we have expressed χ in cgs units, the effective exchange-coupling constant, J_χ (see below), is given in wavenumbers, and T in Kelvin. Equation 1 gives the first two terms of a series expansion in J_χ/k_BT (see Supporting Information) and provides an excellent description of the difference data. The first term of eq 1 is the Curie constant for the Gd^{III} ion ($S_{Gd} = 7/2$); the second term describes low temperature behavior of curve B and depends exclusively on the effective intramolecular exchange constant J_χ. The drop in curve B for $T \rightarrow 0$ indicates that the intramolecular exchange coupling in **6** is antiferromagnetic ($J > 0$). The solid curves in Figure 4 are fits with function $c_1 - c_2/T$, using c_1 and c_2 as adjustable parameters. The inset of Figure 4 shows that this hyperbolic function gives an accurate description of the low temperature section of curve B. The latter fit yields the values $c_1 = 7.865$, which is in excellent agreement with the constant term in eq 1, and $c_2 = 2.6337$, from which we obtain the value $J_\chi = c_2/5.665 = 0.47\ cm^{-1}$ (eq 1). The J_χ value is small, thus the condition $|J_\chi/k_BT| \ll 1$ for the validity of eq 1 is satisfied for the temperatures considered in Figure 4 ($T \geq 5$ K). J_χ value depends slightly on the choice of the temperature range used for the fit and has values ranging from 0.33 cm^{-1} to 0.47 cm^{-1}; for details, see Table S1 of the Supporting Information. A fit of the uncorrected, $\chi_{FeGd}T$ data with the same function (Supporting Information, Figure S6) yields an only marginally higher value for J_χ (0.48 cm^{-1}), which shows that the intermolecular exchange between the irons ($J_{FeFe'}$) has a barely observable effect on the data (the shortest Fe···Fe′ distance in **6** is 9.0 Å).

In the case that the exchange interaction is isotropic with coupling constant J_{iso} and the g-values for both the Fe and Gd are equal to 2, the effective J_χ parameter in eq 1 is equal to the exchange parameter, $J_\chi = J_{iso}$. In the general case that both the exchange and g-values are anisotropic, the effective exchange parameter in eq 1 is given by

$$J_\chi = \frac{1}{12}(g_{1,x}g_{2,x}J_x + g_{1,y}g_{2,y}J_y + g_{1,z}g_{2,z}J_z) \qquad (2)$$

where $g_{1,\xi}$ and $g_{2,\xi}$ ($\xi = x, y, z$) are the g-values for Fe and Gd (section I of Supporting Information). Thus, χT versus T fits using isotropic exchange and Zeeman ($g = 2$) operators do not yield the isotropic part of the exchange-coupling tensor,

$$J_{iso} = \frac{1}{3}(J_x + J_y + J_z) \qquad (3)$$

but the quantity defined in eq 2. As a corollary, it is impossible to determine the individual components J_x, J_y, and J_z from the magnetic susceptibility data for a randomly oriented sample. J_{iso} can be determined provided the coefficients of J_x, J_y, and J_z in eq 2 are equal to a known value. However, J_{iso} eludes determination if the coefficients have different values (as in **6**, see below), even in the case that one has prior knowledge of the g-values. This is a genuine concern because the iron site in **6** has most likely a highly anisotropic set of g-values. For this reason we propose ^{57}Fe Mössbauer spectroscopy as an alternative approach toward determining the exchange parameters of the [FeGd] complex (section 3.5).

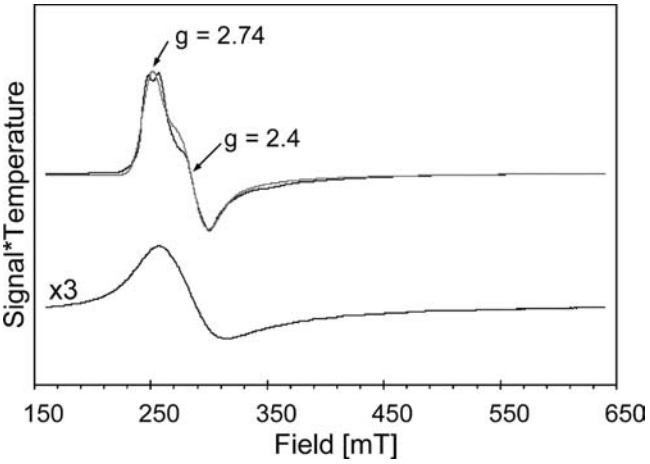

Figure 5. X-band EPR spectra obtained in transversal mode for a [FeLa] sample prepared by precipitation. The simulation for an effective $S = 1/2$ is shown by the gray line (top) and was obtained using: $g_x = 2.74(1)$, $g_y = 2.42(4)$ without g_z ($g_z \sim 0.9$; see the discussion) such that $\sigma_{gx} = 0.084$, $\sigma_{gy} = 0.099$. Experimental conditions: $T = 2.4$ K (top) and $T = 35.2$ K (bottom), 9.65 GHz, 0.99 mT modulation amplitude and 2 mW microwave power.

3.3. Investigation of the Local Fe^{III} $S = 1/2$ Site. 3.3.1. EPR Spectroscopy of [FeLa] Complex. The X-band EPR spectra of an [FeLa] sample obtained by precipitation were recorded at temperatures between 2 and 50 K. Figure 5 shows two representative spectra, taken at 2.4 and 35.2 K. The EPR signal reveals an anisotropic Kramers doublet with $g_x = 2.74 \pm 0.01$, $g_y = 2.42 \pm 0.04$ (shown by arrows). The third component of the g tensor g_z is basically unknown. This resonance could lie either outside or near the limit of our instrument (typically $\nu \sim 9.62$ GHz such that $g_{min} \sim 0.86$ at $B_{max} = 800$ mT). Another possibility is that this resonance is broadly distributed as to be indistinguishable from the background.[21] For the latter case our simulations place an upper limit for this resonance of ~2.0. The g values for [FeLa] are similar to those reported for ferricyanide.[16] In the low temperature range, 2−12 K, the absorption at low field, $g_x = 2.74$, shows an additional splitting of ~10 mT. This splitting could be due to the presence of two distinct iron sites per unit cell, although the two sites are indistinguishable by Mössbauer. The splitting is indiscernible in the 35.2 K spectrum as a result of relaxational line broadening.

3.3.2. ^{57}Fe Mössbauer Spectroscopy of [FeLa] Complex. An [FeLa] sample from the same preparation as the one used for EPR was studied with Mössbauer spectroscopy. The Mössbauer spectra were recorded between 2 and 140 K in magnetic fields up to 8 T.

(21) In special cases, small distortions of the molecular structure can lead to large distributions in the observed g-values. Such a special case has been identified and presented: Stoian, A. S.; Smith, J. M.; Holland, P. L.; Münck, E.; Bominaar, E. L. *Inorg. Chem.* **2008**, *47*(19), 8687.

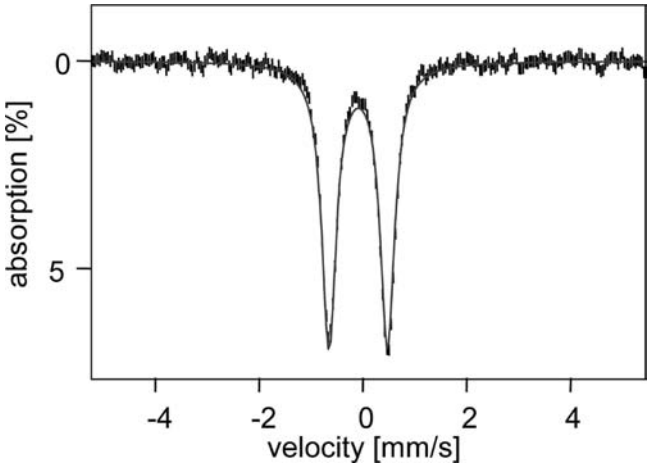

Figure 6. Mössbauer spectra recorded at 150 K in a field of 0.05 T applied parallel to the observed γ-radiation.

The 150 K spectrum of Figure 6 consists of a quadrupole doublet with narrow Lorentzian lines ($\Gamma = 0.31$ mm/s, full width at half-maximum), quadrupole splitting $\Delta E_Q = 1.12 \pm 0.02$ mm/s, and isomer shift $\delta = -0.09 \pm 0.01$ mm/s. The quadrupole splitting, ΔE_Q, is slightly temperature dependent (1.28 mm/s at 50 K and 1.22 mm/s at 100 K), indicating the presence of a low−lying, thermally accessible, excited orbital state.

The 4.2 K spectra recorded in applied fields greater than 2.0 T, shown in Figure 7, demonstrate that the spin system of the Fe^{III} is in the slow relaxation limit. Moreover, at 4.2 K in weak applied fields, for example, $B = 50$ mT, the spectra are broadened by relaxation processes (spectra not shown).

The variable-temperature, variable-field Mössbauer spectra were analyzed, using the WMOSS software, in the framework of a fictitious $S = 1/2$ spin Hamiltonian

$$\hat{\mathcal{H}}_{\mathrm{Fe}} = \hat{\mathcal{H}}_Q + \beta \mathbf{B}\cdot \mathrm{g}\cdot\hat{\mathbf{S}} - \mathrm{g_n}\beta_\mathrm{n}\mathbf{B}\cdot\hat{\mathbf{I}} + \hat{\mathbf{S}}\cdot A\cdot\hat{\mathbf{I}} \qquad (4a)$$

$$\hat{\mathcal{H}}_Q = \frac{eQV_{z'z'}}{12}\left[3\hat{I}_{z'}^2 - \frac{15}{4} + \eta(\hat{I}_{x'}^2 - \hat{I}_{y'}^2)\right] \qquad (4b)$$

$$\Delta E_Q = \frac{eQV_{z'z'}}{2}\sqrt{1+\frac{\eta^2}{3}} \qquad (4c)$$

The terms in eq 4a describe, respectively, the nuclear quadrupole coupling (see eq 4b), electronic and nuclear Zeeman interactions, and the ^{57}Fe magnetic hyperfine interaction. $\hat{\mathbf{S}}$ is the electronic spin of iron, $\hat{\mathbf{I}}$ is the spin of the iron nucleus, and $\mathbf{B}$ is the applied magnetic field. The quadrupole splitting, observed in the absence of magnetic interactions, is given by eq 4c.[22]

The thermal spin expectation value decays as a function of temperature according to a Curie law ($\sim 1/T$) and nearly vanishes at 140 K such that $\mathbf{B}_{\mathrm{int}} \sim 0$. Therefore the pattern observed for the 140 K, 8 T spectrum (Figure 7) is the result of the combined nuclear Zeeman and quadrupole interaction, and affords the determination of the asymmetry parameter of the EFG tensor, $\eta \approx 1$. With this

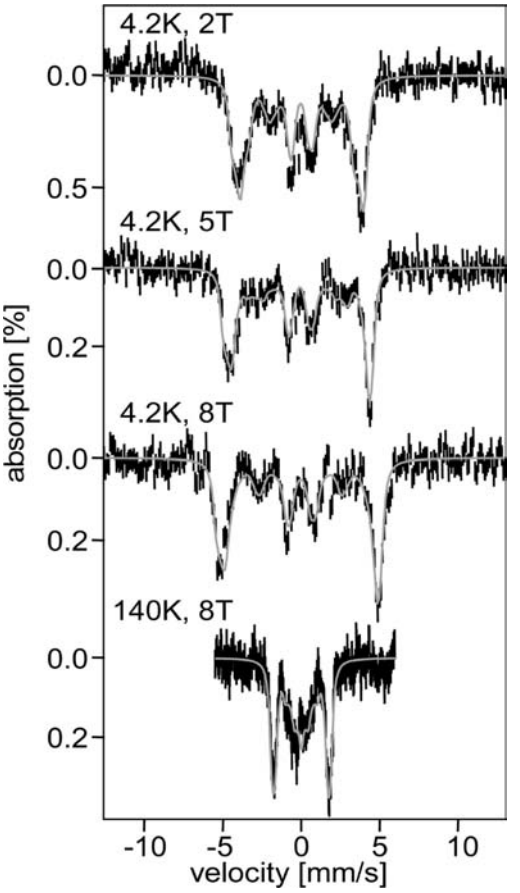

Figure 7. Variable field Mössbauer spectra recorded at 4.2 K in parallel fields of 2 T, 5 T, 8 T and at 140 K in 8 T field. The solid gray lines represent simulations obtained for $S = 1/2$ using the g values as obtained from the X-band EPR spectra ($g_x = 2.74$; $g_y = 2.42$, $g_z = 0.9$), a rotated EFG tensor ($\alpha_{\mathrm{EFG}}=0°$, $\beta_{\mathrm{EFG}}=45°$, and $\gamma_{\mathrm{EFG}}=60°$), and the magnetic hyperfine constants $A_x = +42.5$ T, $A_y = +49.1$ T, and $A_z = +10.0$ T. Simulations for the 4.2 K spectra were computed in slow relaxation, while the simulation for the 140 K spectrum was generated in the fast relaxation regime.

information at hand, we simulated the 4.2 K, high-field spectra to obtain the magnetic hyperfine parameters. Inspection of the spectra presented in Figure 7 shows that the magnetic splitting between the two outer lines increases as a function of increasing applied magnetic field. This behavior indicates that the internal field $\mathbf{B}_{\mathrm{int}}$, is approximately parallel to the externally applied magnetic field $\mathbf{B}$. Since the spectrum associated with the Zeeman ground state ($M = -1/2$) constitutes the principal spectral component of the low temperature spectra, the A values must be (predominantly) positive. Assuming the g and A tensors to be collinear, numerical simulations yield $A_x = +42.5 \pm 0.5$ T, $A_y = +49.0 \pm 0.5$ T and $A_z = +10.0 \pm 5$ T.[23] Finally, to reproduce the relative intensities of the outer lines, the EFG tensor had to be rotated with respect to the g-tensor such that the associated Euler angles are $\alpha_{\mathrm{EFG}} = 0°$, $\beta_{\mathrm{EFG}} = 45 \pm 5°$, and $\gamma_{\mathrm{EFG}} = 60 \pm 10°$.

3.4. Investigation of the Gd^{III} $S = 7/2$ Site by EPR Spectroscopy of the [CoGd] Complex. Spin Hamiltonian parameters of the Gd^{III} site in [FeGd] were obtained from X-band EPR spectra recorded for a sample of [CoLa]

(22) Gütlich, P.; Link, R.; Trautwein, A. X. *Mössbauer Spectroscopy and Transition Metal Chemistry − Inorganic Chemistry Concepts 3*; Springer-Verlag: Berlin, 1978.

(23) (a) Oosterhuis, W. T.; Lang, G. *Phys. Rev.* **1969**, *178*(2), 439. (b) Ono, K.; Shinohara, M.; Ito, A.; Suenaga, M. *Phys. Rev. Lett.* **1970**, *24*(14), 770.

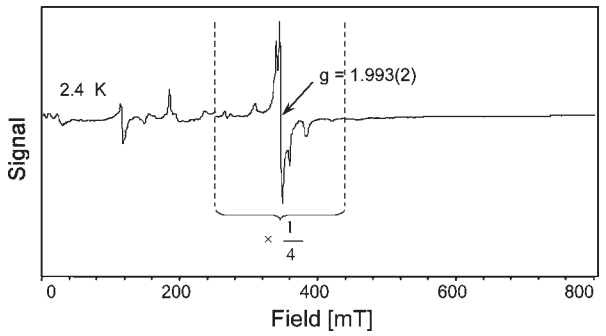

Figure 8. X-band EPR spectrum of the [CoGd] sample recorded at 2.4 K. Experimental conditions: microwave frequency, 9.655 GHz; microwave power, 0.2 mW, and 0.43 mT modulation amplitude. For clarity the intensity in the central section has been reduced by a factor 4 relative to the outer region. The central region is shown separately in Figure 9.

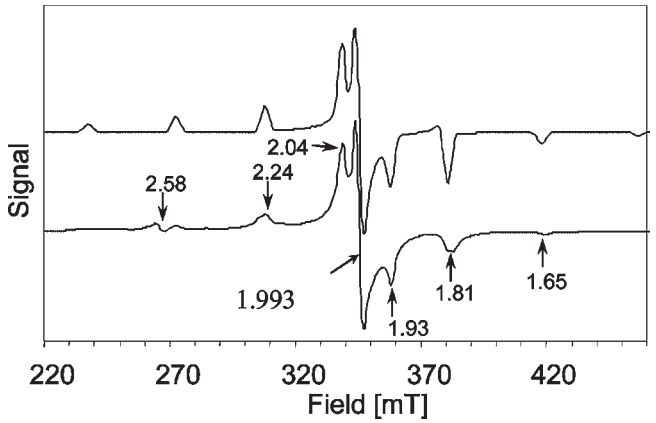

Figure 9. X-band EPR spectrum of [CoGd] recorded at 2.4 K (expanded region from Figure 8). Above the data is shown a simulation based on eq 5 using $g = 1.993$, $D = +0.0182$ cm^{-1}, and $E/D = 0.31$.

doped with 1% Gd^{III}: $[CoLa_{1-x}Gd_x]_{x=0.01}$. The sample used here was obtained by co-precipitation of an appropriate mixture of lanthanide salts with cobalticyanide. This sample allowed us to study the Gd^{III} sites in magnetically isolated form, as the Co^{III} and La^{III} sites are diamagnetic and the magnetic isolation of the Gd^{III} sites is sufficient to eliminate spin−spin interactions. In accordance with earlier studies of Gd^{III} complexes,[24] we observed an EPR signal that shows well resolved fine structure with dominant features centered around $g = 2$ (Figure 8). While some of the features in the low field region are lost by increasing the temperature, the $g = 2$ region retains most of its spectral resolution, and the quantity (signal intensity × temperature) is, within the error margin, constant in the explored 2.4−60 K range, suggesting that excited states are not measurably populated.

Gd^{III} has a $4f^7$ electronic configuration with an $^8S_{7/2}$ ground state: The central derivative EPR feature at $g = 1.993(2)$ (Figure 8) is due to the $-1/2 \leftrightarrow +1/2$ transition. The other $|\Delta M| = 1$ transitions, $+1/2 \leftrightarrow +3/2$, ..., $+5/2 \leftrightarrow +7/2$ and $-1/2 \leftrightarrow -3/2$, ..., $-5/2 \leftrightarrow -7/2$ appear with increasing displacements as a function of M to the left and the right of the $-1/2 \leftrightarrow +1/2$ transition (Figure 9). The displacements from $g = 2$ result from small zero-field splittings (ZFS) of the ground multiplet, induced by spin−orbit coupling of the ground state with excited crystal-field states. In earlier studies of Gd^{III} in rhombic coordination,[24] the largest contributions to the ZFS were identified as those pertaining to the quadratic terms (parameters D and E) of the spin Hamiltonian. We have analyzed the $|\Delta M| = 1$ transitions with the $S = 7/2$ Hamiltonian.

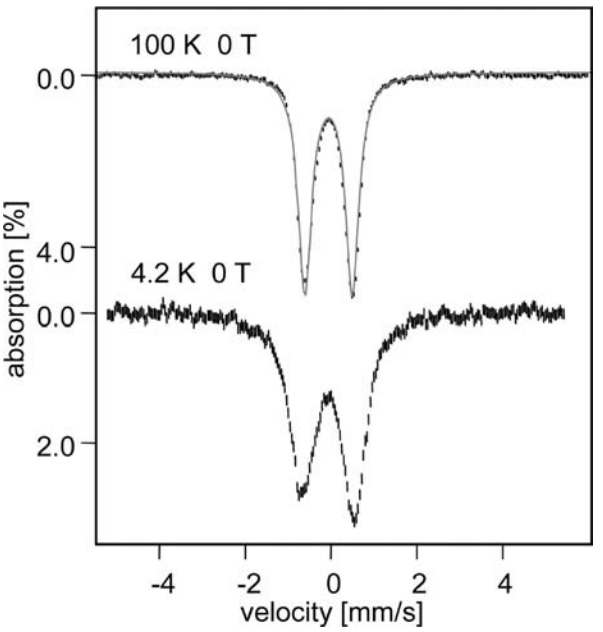

Figure 10. Mössbauer spectra recorded for the [FeGd] sample in zero field at 100 K (top) and 4.2 K (bottom).

$$\hat{\mathscr{H}}_{Gd} = g\beta\mathbf{B}\cdot\hat{\mathbf{S}} + D\left[\hat{S}_z^2 - \frac{1}{3}S(S+1) + \frac{E}{D}(\hat{S}_x^2 - \hat{S}_y^2)\right] \quad (5)$$

Figure 9 shows the 2.4 K spectrum in the field range containing the $|\Delta M| = 1$ transitions and a representative SpinCount simulation based on eq 5. Good agreement with experiment is obtained for $D \sim 0.02$ cm^{-1} and a nearly rhombic $E/D \approx 1/3$.

In the $g = 2$ region the Zeeman splitting dominates the splitting of the spin levels. In the low-field region the Zeeman energy is comparable to the zero field splitting, resulting in extensive level mixing. Extending our simulations with the spin Hamiltonian of eq 5 to the low-field range yielded a number of weak transitions which, however, did not match well the observed features, possibly because the low-field resonances are more susceptible to quartic and higher order terms of the spin Hamiltonian.

3.5. Study of the Exchange Interaction in [FeGd] with ^{57}Fe Mössbauer Spectroscopy. We have recorded Mössbauer spectra for [FeGd] in applied fields up to 8 T at temperatures ranging from 4.2 to 150 K for two samples, one of which obtained by precipitation and the other prepared by grinding crystals. Since both samples yielded essentially the same spectra, we focus here on the

(24) (a) Reynolds, R. W.; Boatner, L. A. *J. Chem. Phys.* **1972**, *56*(11), 5607. (b) Jones, D. A.; Baker, J. M.; Pope, D. F. D. *Proc. Phys. Soc.* **1959**, *74*(3), 249. (c) Kliava, J.; Edelman, I. S.; Potseluyko, A. M.; Petrakovskaja, E. A.; Berger, R.; Bruckental, I.; Yeshurun, Y.; Malakhovskii, A. V.; Zarubina, T. V. *J. Phys.: Condens. Matter* **2003**, *15*, 6671. (d) Clarkson, R. B.; Smirnov, A. I.; Smirnova, T. I.; Kang, H.; Belford, R. L.; Earle, K.; Freed, J. H. *Mol. Phys.* **1998**, *95*(6), 1325.

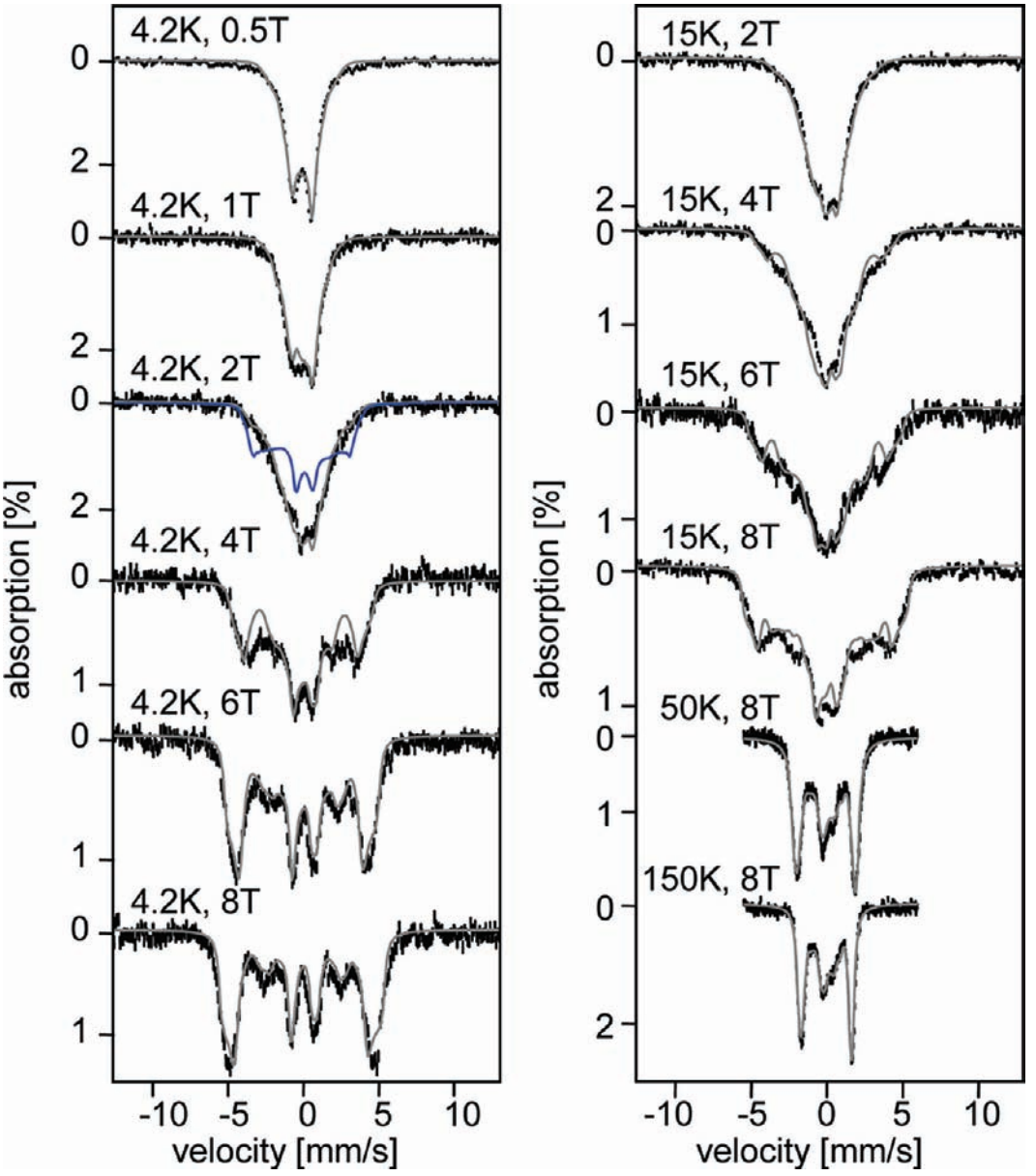

Figure 11. Field dependence of the Mössbauer spectra recorded for the [FeGd] sample at 4.2 K (left panel) and 15 K (right panel, top) as well as the spectra recorded in 8 T at 50 and 150 K (right panel, bottom). The solid gray lines are simulations obtained using the spin Hamiltonian of eq 6 and the parameters presented in Table 6 such that $J_x = 0.11$, $J_y = 0.33$, and $J_z = 1.2\ \mathrm{cm}^{-1}$. The solid blue line shown for the 4.2 K, 2.0 T spectrum presents a simulation under conditions, $T_{\mathrm{set}} = 0.05$ K, for which only the lowest magnetic level of the spin manifold is populated (see text).

sample obtained through precipitation. A zero field spectrum recorded at 100 K (Figure 10, top) consists of a nearly symmetric doublet with $\Delta E_{\mathrm{Q}} = 1.10 \pm 0.02$ mm/s, $\delta = -0.06 \pm 0.01$ mm/s, and line width $\Gamma \approx 0.38$ mm/s, parameters that closely match those of [FeLa]. The 4.2 K spectrum of Figure 10, also taken in zero field, exhibits a broadened doublet with $\Delta E_{\mathrm{Q}} \approx 1.2$ mm/s.[25]

Figure 11 shows a series of spectra recorded between 4.2 and 150 K. These spectra were analyzed in the framework of the spin Hamiltonian

$$\hat{\mathscr{H}}_{\mathrm{FeGd}} = \hat{\mathscr{H}}_{\mathrm{Fe}} + \hat{\mathscr{H}}_{\mathrm{Gd}} + \hat{\mathbf{S}}_{\mathrm{Fe}} \cdot J \cdot \hat{\mathbf{S}}_{\mathrm{Gd}} \qquad (6)$$

which is the sum of the Hamiltonians for the Fe^{III} site (eq 4a) and the Gd^{III} site (eq 5), with an additional term describing the exchange coupling of the two spin systems.

To gain insight into the nature of these spectra, we make use of the susceptibility data which showed that the components of J are on the order of a wavenumber. Under these conditions the Zeeman term dominates the exchange coupling, $2\beta B \approx 8\ \mathrm{cm}^{-1}$ at 8.0 T, and not surprisingly the 4.2 K spectrum strongly resembles its [FeLa] counterpart. Our simulations show that the 8.0 T spectrum essentially reflects the uncoupled Fe site of [FeGd]. However, A_x and A_y are about 5−15% smaller in [FeGd] than in [FeLa]. The x and y components of the A-tensor are positive and reflect a dominant orbital contribution, which is proportional to $(g_{x,y} - 2)$. In this

(25) Presently we do not fully understand the broadening, although, the high density of closely spaced electronic levels may offer an explanation.

Table 6. Spin Hamiltonian (eqs 5 and 6) Parameters Derived from the Analysis of Mössbauer and EPR Spectra

		[FeLa]	[FeGd]
Fe site	g_x	2.74	2.74
	g_y	2.42	2.42
	g_z[a]	*0.9*	*0.9*
	δ [mm/s][b]	-0.09 ± 0.01	-0.06 ± 0.01
	ΔE_Q [mm/s][b]	1.22 ± 0.04	1.10 ± 0.04
	η	~ 1.0	~ 1.36
	α_{EFG} [deg]	0	0
	β_{EFG} [deg]	45 ± 5	35 ± 5
	γ_{EFG} [deg]	60 ± 10	65 ± 3
	A_x [T]	42.5 ± 0.5	37.0 ± 0.5
	A_y [T]	49.0 ± 0.5	51.0 ± 0.5
	A_z [T]	10.0 ± 5.0	0.0 ± 5.0
		[CoLa]	[FeGd]
Co site	D [cm^{-1}]	+ 0.0182	+ 0.02
	E/D	0.31	0.33
	g_{iso}	1.993	2.00
			[FeGd]
exchange coupling		J_x [cm^{-1}][c]	0.1 ± 0.1
		J_y [cm^{-1}][c]	0.3 ± 0.1
		J_z [cm^{-1}][c]	1.2 ± 0.2
		J_{iso} [cm^{-1}][c]	0.55 ± 0.1
		J_χ [cm^{-1}][d]	0.33−0.47

[a] g_z is experimentally undetermined; the value reported here is derived from the theoretical analysis presented in section 4. Moreover, this value has been used in the subsequent analysis of the Mössbauer spectra. [b] Values determined from the zero field spectra recorded at 100 K. [c] Values determined from the analysis of the Mössbauer data. [d] Value determined from analysis of the magnetic susceptibility data, see section 3.2 and Supporting Information.

view the 5% reduction in $A_{x,y}$ corresponds to a reduction in $g_{x,y}$ by only 0.05 relative to [FeLa]. It is noteworthy that the EFG tensor in [FeGd] is similarly rotated as in [FeLa]. These observations suggest for the analysis of the [FeGd] spectra that one can transfer, with slight modifications, the parameters of [FeLa]. Thus, the analysis of the rather complex [FeGd] spectra essentially involves the determination of J.

The 4.2 K spectra shown in the left panel of Figure 11 are exceedingly complex. At 4.2 K the electronic spin of the coupled system relaxes slowly on the time scale of Mössbauer spectroscopy. Consequently, the low field spectra ($B < 3$ T) are a superposition of $(2S_{Gd}+1)\times(2S_{Fe}+1) = 16$ distinct spectra, one for each spin level of the coupled system. Our simulations show that the exchange coupling must be antiferromagnetic and anisotropic with $J_x \approx 0.1$ cm^{-1}, $J_y \approx 0.3$ cm^{-1}, and $J_z \approx 1.2$ cm^{-1} giving the best result. For the quoted anisotropy of J the coupled system has considerable Ising character along z, and thus a description of the system by pure $S = 3$ and $S = 4$ multiplets is inappropriate. The Zeeman interaction with the Fe^{III} is strongest in the plane perpendicular to the direction of J_z. Since the expectation values of $\hat{\mathbf{S}}_{Fe}$, which determine the ^{57}Fe magnetic hyperfine interactions, are different for all levels in weak applied magnetic fields, the low field spectra are not readily described in simple sentences. The coupled spin manifold is a non-Kramers system and thus all

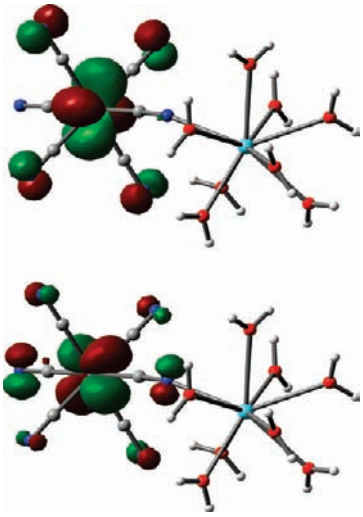

Figure 12. (Top) *xy* orbital, which contains the unpaired electron of the low-spin Fe^{III} site in the ground configuration of the [FeLa] complex. (Bottom) *xz* orbital, which is doubly occupied in the ground configuration and single occupied in one of the excited states.

expectation values of $\hat{\mathbf{S}}_{Fe}$ are zero in the absence of an applied field (unless spin levels approach to closer than 0.01 cm^{-1} and are mixed by magnetic hyperfine interactions),[26] with the consequence that a quadrupole doublet is observed. An increasing applied field competes with the antiparallel exchange coupling and gradually forces $<\hat{\mathbf{S}}_{Fe}>$ to be parallel to $<\hat{\mathbf{S}}_{Gd}>$. The profound changes observed between 2 and 4 T reflect the fact that the increasing Zeeman splitting yields an increased thermal population of the ground state, roughly the $M_{Fe} = -1/2$, $M_{Gd} = -7/2$ product state. The combined action of decoupling the Fe and Gd spins and thermal population of the ground level transforms the spectra, in the progression from 4 to 8 T, into a shape that strongly resembles the magnetically isolated case observed for [FeLa].

We mentioned that the population of 16 electronic states contributes to the shapes of the $B < 3$ T spectra at 4.2 K. To illustrate this point we have calculated a 2 T spectrum (blue line) at $T = 0.05$ K, a temperature for which only the ground level would be thermally populated. Further, the unresolved features of the 2 T, 4.2 K spectrum suggests that it results from a superposition of many Boltzmann-weighted *sub*spectra, showing that the relaxation rate of the electronic spin is slow. In the fast relaxation limit the 2 T, 4.2 K spectrum would have well-defined features as illustrated in Supporting Information, Figure S8 (Spectral simulations of the 8.0 T, 4.2 K and 8.0 T, 15 K spectra show that the relaxation remains slow even at 15 K.)

Initially we focused on simulating the spectra with an isotropic exchange coupling, obtaining $J_{iso} = +0.8$ cm^{-1}. While this parameter gives a reasonable description of the data, given the complexity of the problem, this solution is clearly not perfect (see Supporting Information, Figures S10 and S11). Moreover, the J_{iso} value obtained from the Mössbauer analysis was found to be in conflict with the susceptibility results, which suggested $J_\chi \sim 0.4(1)$ cm^{-1} when the data analysis was restricted to an isotropic exchange interaction. This conflict, together with insights gleaned from a theoretical analysis of the problem,

(26) Sureus, K. K.; Hendrich, M. P.; Christie, P. D.; Rottgardt, D.; Orme-Johnson, W. H.; Münck, E. *J. Am. Chem. Soc.* **1992**, *114*, 8579.

prompted us to search for a solution involving anisotropic exchange. The resulting solution, illustrated by the theoretical curves of Figure 11 and listed in Table 6, provides significantly improved simulations for the entire data set.

4. Discussion

The exchange parameters listed in Table 1 for the Fe(μ-CN)Gd complexes were obtained from simulations of the magnetic susceptibility data on the basis of an isotropic exchange Hamiltonian and isotropic g-values close to 2. Thus, the values obtained represent the effective coupling constant J_χ (eq 2) rather than the isotropic exchange parameter J_{iso} (eq 3) as claimed in the reports.[8b,13c] The difference between J_χ and J_{iso} is likely to be sizable, given that the g-values of low-spin Fe^{III} with cyano coordination are highly anisotropic. For the sake of comparison, we have listed the J_χ value for **6** as obtained from magnetic susceptibility analysis (Supporting Information, Table S1) and not the J_{iso} value of 0.55 cm^{-1} deduced from a Mössbauer analysis. The J_χ values for **6** and the Fe(μ-CN)Gd complex of ref 13c represent weak antiferromagnetic interactions of which the latter is larger in magnitude (see Table 1). The third value listed (-1.5 cm^{-1}) is ferromagnetic but was obtained for a compound exhibiting antiferromagnetic behavior that was attributed[8b] to a prevailing antiferromagnetic coupling between the molecules, $J_{inter} = +0.16$ cm^{-1}.[27] However, as we pointed out earlier, since the contributions to χT arising from weak intra- and intermolecular exchange are indistinguishable, the J_χ value of -1.5 cm^{-1} must be ambiguous.

To determine the electronic structure of the iron sites in **1** and **6** we have performed density functional theory (DFT) calculations for the crystallographic structures of these complexes. The calculations show that the two systems have a t_{2g}^5 ground configuration in which the unpaired electron is accommodated by the *xy* orbital (Figure 12), where the *z* axis is along the cyano bridge and *x* and *y* are aligned along the equatorial bonds. The electronic configuration is similar to the one found for a related Fe(μ-CN)Gd compound in an earlier DFT study,[8b] suggesting that the presence of an Ln^{III} ion as a secondary neighbor affects the crystal field at the iron in a way that lowers the energies of the *yz* and *xz* orbitals relative to that of the *xy* orbital.

The wave functions of the lowest Kramers doublet for the low-spin Fe^{III} site can be expressed as

$$|+\rangle = a|yz^-\rangle + ib|xz^-\rangle + c|xy^+\rangle \quad (7a)$$

$$|-\rangle = -a|yz^+\rangle + ib|xz^+\rangle + c|xy^-\rangle \quad (7b)$$

where *a*, *b*, and *c* are real coefficients. On the basis of our DFT calculations, *c* must have the largest magnitude, and *a* and *b* describe the admixture of the lowest spin−orbitals of the crystal field with spin-reversed excited spin−orbitals due to spin−orbit coupling. The admixtures lead to anisotropic exchange, which can be formulated by the effective Hamiltonian

$$\hat{\mathscr{H}} = J_x\hat{S}_{1,x}\hat{S}_{2,x} + J_y\hat{S}_{1,y}\hat{S}_{2,y} + J_z\hat{S}_{1,z}\hat{S}_{2,z} \quad (8)$$

where $S_1 = 1/2$ (fictitious Fe spin) and $S_2 = 7/2$ (Gd spin). In principle, there arises also an antisymmetric exchange term but this contribution will not be considered here. The coupling constants in eq 8 are given by the expressions[28]

$$J_x = -a^2j_{yz} + b^2j_{xz} + c^2j_{xy} \quad (9a)$$

$$J_y = +a^2j_{yz} - b^2j_{xz} + c^2j_{xy} \quad (9b)$$

$$J_z = -a^2j_{yz} - b^2j_{xz} + c^2j_{xy} \quad (9c)$$

Exchange parameter j_d (d = *yz*, *xz*, *xy*) represents the average coupling of an unpaired electron in 3d orbital d at Fe with the seven unpaired 4f electrons at Gd:

$$j_d = \frac{1}{7}\sum_{i=1}^{7} j_{d,f_i} \quad (10)$$

$j_{d,f}$ is the exchange-coupling constant, using the same $j\hat{\mathbf{s}}_1\cdot\hat{\mathbf{s}}_2$ convention ($s_1 = s_2 = 1/2$) as in eqs 8 and 9a−9c, for the pathway between 3d orbital d and 4f orbital f.

The g-values for the Kramers doublet in eqs 7a−7b are given by the expressions

$$g_x = -2a^2 + 2b^2 + 2c^2 + 4kbc \quad (11a)$$

$$g_y = +2a^2 - 2b^2 + 2c^2 + 4kac \quad (11b)$$

$$g_z = -2a^2 - 2b^2 + 2c^2 - 4kab \quad (11c)$$

where *k* is the covalent reduction factor of the orbital term in the Zeeman operator, $\mu_B\mathbf{H}\cdot(k\hat{\mathbf{L}} + 2\hat{\mathbf{S}})$.

Let us first consider the ionic case, $k = 1$. In principle, the coefficients *a*, *b*, and *c* in eqs 7a−7b and 9a−9c can be determined from the g-values of the [FeLa] complex **1**. However, as mentioned in section 3.3.1, EPR analysis of **1** yields only two of the three g-values, namely, 2.74 and 2.42. There are six ways to assign the two known g-values to g_x, g_y, and g_z of eqs 11a−11c. Each assignment results in two equations, which in combination with the normalization condition for the states in eqs 7a−7b, affords solutions for *a*, *b*, and *c* . The only way to get a solution in which *c* appears as the coefficient with the largest magnitude is by assigning the two experimental g-values to g_x and g_y. The resulting equations $g_x(a,b,c) = 2.74$, $g_y(a,b,c) = 2.42$, and $a^2 + b^2 + c^2 = 1$ give two solutions: $a = 0.424$, $b = 0.472$, $c = 0.773$ (solution 1) and $a = 0.158$, $b = 0.218$, $c = 0.963$ (solution 2). Equations 11a−11c provide the value of the undetermined g-value: $g_z = -0.41$ for solution 1 and $g_z = 1.57$ for solution 2. In the Mössbauer simulations for [FeGd] complex **6** the smallest g-value (g_z) was associated with the direction with the largest exchange coupling ($J_z = 1.20$ cm^{-1}), the largest g-value ($g_x = 2.74$) with the smallest coupling ($J_x = 0.11$ cm^{-1}), and consequently $g_y = 2.42$ with $J_y = 0.33$ cm^{-1}. Substitution of the experimental values for J_x, J_y, and J_z into eqs 9a−9c, gives a set of linear equations for the quantities a^2j_{yz}, b^2j_{xz}, and c^2j_{xy}, yielding the solutions -0.435 cm^{-1}, -0.545 cm^{-1}, and $+0.220$ cm^{-1}, respectively. By substituting the values for *a*, *b*, and *c* derived from the g-values, we obtain $j_{yz} = -2.42$ cm^{-1}, $j_{xz} = -2.44$ cm^{-1}, and $j_{xy} = +0.37$ cm^{-1} for solution 1 and $j_{yz} = -17.3$ cm^{-1}, $j_{xz} = -11.4$ cm^{-1}, and $j_{xy} = +0.24$ cm^{-1} for solution 2.

Let us now consider the covalent case, $k < 1$. The first three terms in the expressions for the g-values (eqs 11a−11c) originate from the $2\hat{\mathbf{S}}$ term in the Zeeman operator and yield sums ≤ 2 as can readily be seen from the expressions.

(27) This coupling is much smaller than J_{intra} but has a large effect on χT because it acts between large dimer spins, $S = 3$ or 4.

(28) Bencini, A.; Gatteschi, D. *Mol. Phys.* **1982**, *47*, 161.

The inequality is rooted in the mixing of spin up and down terms in the wave functions in eqs 7a−7b. Only the fourth term, which arises from the orbital term $\hat{\mathbf{L}}$ of the Zeeman operator, gives contributions that may lead to g-values in excess of 2. Hence, there exists for any two g-values with magnitudes larger than 2 a value for k, denoted k_0, below which eqs 11a−11c have no solutions for a, b, and c. For the g-values 2.74 and 2.42 of the [FeLa] complex, **1**, the value is $k_0 = 0.8689$. When the orbital term in the Zeeman operator is gradually quenched by decreasing k below 1, then the g_z value for the solution with the smallest g_z value (solution 1) increases, and the g_z for the solution with the largest g_z value (solution 2) decreases, which eventually leads to a merging of the two solutions into a single solution with $g_z = 0.935$ and $a = 0.275, b = 0.333, c = 0.902$ at $k = k_0 = 0.8689$ (solution 3). Solution 3 gives the values $j_{yz} = -5.74$ cm^{-1}, $j_{xz} = -4.92$ cm^{-1}, and $j_{xy} = +0.27$ cm^{-1}.

All three solutions yield ferromagnetic j_{yz} and j_{xz} couplings and an antiferromagnetic j_{xy}. The coupling constant for the ground orbital xy is much weaker than for the two excited orbitals, $j_{xy} \ll |j_{yz}| \approx |j_{xz}|$, which can be rationalized by noting that xy has no cyano-bridge orbital of matching symmetry to interact with, in contrast to yz and xz which can mix with π orbitals of the bridge, leading to a stronger super exchange type of interaction. This property is illustrated by the contour plots for the xy and xz orbitals (Figure 12) obtained by DFT calculations for the [FeLa] complex, **1**, of which only the latter is visibly delocalized toward the bridging ligand. The mechanistic origins of the exchange interactions in **6** will be the subject of a future report. The j_{yz} and j_{xz} values for solution 1 and 3 have similar magnitudes as the J values listed in Table 1; the values for solution 2 are much larger in magnitude, exceeding the observed J values, including those for the Cu(μ-O)$_2$Gd complexes. The exchange parameter for the orbital carrying the largest spin population, j_{xy}, is smaller than the isotropic exchange parameter,

$$J_{iso} = -\frac{1}{3}a^2 j_{yz} - \frac{1}{3}b^2 j_{xz} + c^2 j_{xy} \qquad (12)$$

because of a positive contribution from the first two terms, which more than offsets the reduction of the j_{xy} term by c^2.

The expression $\chi_{FeLa}T = (g_x^2 + g_y^2 + g_z^2)/32$ cm^3 mol^{-1} K obtained in the limit $T \rightarrow 0$ yields the values 0.423, 0.495, and 0.445 cm^3 mol^{-1} K for solutions 1, 2, and 3, respectively, and reveals that the solutions with low g_z values (solutions 1 and 3) are in much better agreement with the experimental value ($\chi_{FeLa}T \approx 0.44(2)$ cm^3 mol^{-1} K at 4 K) than the one with the largest g_z value (solution 2). To calculate the $\chi_{FeLa}T$ versus T plot for each of the solutions, we have interpreted the g-values in terms of a crystal-field model for the t_{2g}^5 states with energies ε_{yz}, ε_{xz}, and ε_{xy} (the subscript indicates the orbital containing the unpaired electron) and 1-electron spin−obit coupling constant ζ. The g-values for **1** imply energies that appear in the order $\varepsilon_{yz} > \varepsilon_{xz} > \varepsilon_{xy}$. Obviously, the coefficients a, b, and c, and by consequence the g-values, are a function of the ratios $(\varepsilon_{yz} - \varepsilon_{xy})/\zeta$ and $(\varepsilon_{xz} - \varepsilon_{xy})/\zeta$. Adopting the value $\zeta = 250$ cm^{-1}, typical for ferricyanide,[29] we obtained for the crystal-field splittings $\varepsilon_{yz} - \varepsilon_{xy}$ and $\varepsilon_{xz} - \varepsilon_{xy}$ the values 222 cm^{-1} and 172 cm^{-1} (solution 1), 883 cm^{-1} and 593 cm^{-1} (solution 2), and 414 cm^{-1} and 311 cm^{-1} (solution 3). Using these splittings, we have evaluated the $\chi_{FeLa}T$ versus T curves shown in Figure S7 of the Supporting Information. The curve for solution 1 has a much steeper slope than observed, the slope for solution 2 is too gentle, and solution 3 reproduces the observed slope. The slopes reflect the size of the crystal-field splittings, with a small splitting corresponding to a steep slope and vice versa. The slopes for solutions 1 and 2 can be adjusted to the observed slope, without changing the value in the low-temperature limit, by scaling the two crystal-field splittings and ζ with a common factor. However, this procedure leads to a value for ζ of ∼500 cm^{-1} in the case of solution 1, which is larger than the free ion value of 400 cm^{-1} and obviously too large, and to a ζ value of ∼125 cm^{-1} in the case of solution 2, which is unacceptably small. Thus, solution 3 is clearly the preferred one from the perspective of the magnetic susceptibility analysis and is compatible with the Mössbauer analysis. The covalent reduction factor for solution 3 is virtually equal to the value $k = 0.87$ reported for $K_3[Fe(CN)_6]$ dispersed in $K_3[Co(CN)_6]$,[30] lending additional support to this solution.

The exchange couplings for the Cr(μ-CN)Gd bridges listed in Table 1 are most likely isotropic, owing to the half-filled t_{2g}^3 shell of the Cr^{3+} ion, and can be expressed as $J_{CrGd} = (j_{yz} + j_{xz} + j_{xy})/3$. Assuming that the exchange parameters for the 3d orbitals of the Fe(μ-CN)Gd bridge in **6** are transferable to Cr(μ-CN)Gd, J_{CrGd} is predicted to be −1.5 cm^{-1} for solution 1, −9.5 cm^{-1} for solution 2, and −3.4 cm^{-1} for the preferred solution 3. The values based on solutions 1 and 3 provide the best match with the magnitudes of the J values listed for Cr(μ-CN)Gd bridges in Table 1. The predicted couplings are ferromagnetic while the observed couplings for this type of bridge (Table 1) can be of either sign, suggesting that the transferability assumption is not warranted, even between compounds with the same bridging unit. Factors that may influence the exchange coupling are the metric parameters of the bridging unit, which vary among these systems.

After having determined the g-values of the two paramagnetic sites in **6**, we can verify if the exchange parameters obtained for this complex by Mössbauer spectroscopy are consistent with the magnetic susceptibility data. Let us first consider the value $J_{iso} = 0.8$ cm^{-1}, which was obtained from the only partly satisfactory spectral simulations with an isotropic exchange Hamiltonian (section 3.5.). Substitution of this value and the g-values into eq 2 yields $J_\chi = 0.63$ cm^{-1} for solution 1, 0.90 cm^{-1} for solution 2, and 0.81 cm^{-1} for solution 3. These values are much larger than the J_χ values, ranging from 0.33 cm^{-1} to 0.47 cm^{-1} (Supporting Information, Table S1), obtained from the magnetic susceptibility analysis. Thus, the assumption of isotropic exchange leads to inconsistent values for J_χ as obtained by different techniques and therefore must be rejected. Let us now consider parameters $J_x = 0.11$ cm^{-1}, $J_y = 0.33$ cm^{-1}, and $J_z = 1.20$ cm^{-1} obtained from the successful simulations of the Mössbauer spectra on the basis of an anisotropic exchange Hamiltonian. Substitution of these values and the g-values into eq 2 yields $J_\chi = 0.10$ cm^{-1} for solution 1, 0.50 cm^{-1} for solution 2, and 0.37 cm^{-1} for solution 3. The J_χ value for solution 1 lies clearly outside the range deduced from the magnetic susceptibility analysis, the J_χ for solution 2 is at its upper fringe, and the value for solution 3 is inside this range. This result corroborates solution 3 as the preferred solution. We notice that while the J_χ values for the three solutions are obtained with the same set of values for the

(29) Jackson, L. C. *Proc. Phys. Soc.* **1938**, *50*, 707.

(30) Abragam, A.; Bleaney, B. *Electron Paramagnetic Resonance of Transition Ions*; Dover, NY, 1986; p 482.

anisotropic parameters, they all differ from the isotropic exchange parameter $J_{iso} = (J_x + J_y + J_z)/3 = 0.55\ cm^{-1}$. This study adds to the evidence[31] that exchange interactions between transition metal ions and gadolinium can be anisotropic.

Acknowledgment. This research was supported by the U.S. NIH (EB001475 to E.M.). Financial suport by the CNCSIS (PNII − IDEI-1912/2009) is gratefully acknowledged.

(31) Yan, Y.; Xu, S. W.; Jin, H. M.; Du, X. B.; Su, F. *Chin. Phys.* **2004**, *13*, 1965.

Supporting Information Available: Details of the analysis of the magnetic susceptibilities, the derivation of eqs 1 and 2 as well as a proof for the validity of the subtraction method in the analysis of χT versus T of [FeGd] are presented. Complete crystallographic data, structure, solution, and refinement are available. This material is available free of charge via the Internet at http://pubs.acs.org.